Usp25m protease regulates ubiquitin-like processing of TUG proteins to control GLUT4 glucose transporter translocation in adipocytes

Received for publication, March 20, 2018, and in revised form, May 9, 2018 Published, Papers in Press, May 17, 2018, DOI 10.1074/jbc.RA118.003021

Estifanos N. Habtemichael[‡], Don T. Li[‡§1], Abel Alcázar-Román[‡], Xavier O. Westergaard[‡], Muyi Li[‡], Max C. Petersen[‡¶2], Hanbing Li[‡‖], Stephen G. DeVries[‡], Eric Li[‡], Omar Julca-Zevallos[‡§], Joseph S. Wolenski[**], and Jonathan S. Bogan[‡§3]

From the [‡]Section of Endocrinology and Metabolism, Department of Internal Medicine and the Departments of [§]Cell Biology and [¶]Cellular and Molecular Physiology, Yale University School of Medicine, the [**]Department of Molecular, Cellular and Developmental Biology, Yale University, New Haven, Connecticut 06520, and the [‖]Institute of Pharmacology, Department of Pharmaceutical Sciences, Zhejiang University of Technology, Hangzhou 310014, China

Edited by Jeffrey E. Pessin

Insulin stimulates the exocytic translocation of specialized vesicles in adipocytes, which inserts GLUT4 glucose transporters into the plasma membrane to enhance glucose uptake. Previous results support a model in which TUG (Tether containing a UBX domain for GLUT4) proteins trap these GLUT4 storage vesicles at the Golgi matrix and in which insulin triggers endoproteolytic cleavage of TUG to translocate GLUT4. Here, we identify the muscle splice form of Usp25 (Usp25m) as a protease required for insulin-stimulated TUG cleavage and GLUT4 translocation in adipocytes. Usp25m is expressed in adipocytes, binds TUG and GLUT4, dissociates from TUG-bound vesicles after insulin addition, and colocalizes with TUG and insulin-responsive cargoes in unstimulated cells. Previous results show that TUG proteolysis generates the ubiquitin-like protein, TUGUL (for TUG ubiquitin-like). We now show that TUGUL modifies the kinesin motor protein, KIF5B, and that TUG proteolysis is required to load GLUT4 onto these motors. Insulin stimulates TUG proteolytic processing independently of phosphatidylinositol 3-kinase. In nonadipocytes, TUG cleavage can be reconstituted by transfection of Usp25m, but not the related Usp25a isoform, together with other proteins present on GLUT4 vesicles. In rodents with diet-induced insulin resistance, TUG proteolysis and Usp25m protein abundance are reduced in adipose tissue. These effects occur soon after dietary manipulation, prior to the attenuation of insulin signaling to Akt. Together with previous data, these results support a model whereby insulin acts through Usp25m to mediate TUG cleavage, which liberates GLUT4 storage vesicles from the Golgi matrix and activates their microtubule-based movement to the plasma membrane. This TUG proteolytic pathway for insulin action is independent of Akt and is impaired by nutritional excess.

Upon insulin stimulation, fat and muscle cells recruit specialized vesicles containing GLUT4 (glucose transporter 4) glucose transporters to the cell surface (1). These "GLUT4 storage vesicles" (GSVs)[4] are sequestered intracellularly in unstimulated cells, so that GLUT4 is excluded from the plasma membrane, and glucose uptake is restricted. Insulin mobilizes the GSVs to insert GLUT4 at the cell surface, thus promoting glucose uptake from the circulation. Also called "insulin-responsive vesicles," GSVs are distinct from endosomes and are thought to exist as a preformed pool in cells not stimulated with insulin (2). In addition to GLUT4, GSVs contain specific cargo proteins, including IRAP (insulin-responsive aminopeptidase) and LRP1 (low-density lipoprotein receptor-related protein 1), and they are formed in a cell type–specific manner by the action of sortilin and other proteins that couple cargo recruitment to vesicle budding (3–5). In primary adipocytes, insulin-stimulated GSV mobilization can cause a 20–30-fold increase in cell-surface GLUT4 and glucose uptake. How GSVs are regulated by insulin is not well-understood.

The TUG protein is a functional Tether, containing a ubiquitin-like UBX domain, for GLUT4, which traps GLUT4 intracellularly in unstimulated cells and releases GLUT4 upon insulin stimulation (6, 7). Identified initially in a genetic screen, TUG was proposed to act specifically on GSVs and not at other sites of GLUT4 trafficking. Subsequent data further support this view and show that TUG-regulated vesicles display the kinetic properties, cargo specificity, cell-type specificity, diam-

This work was supported, in whole or in part, by National Institutes of Health Grant R01 DK092661 (to J. S. B.) and by American Diabetes Association Grant 1-17-IBS-40 (to J. S. B.). The authors declare that they have no conflicts of interest with the contents of this article. The content is solely the responsibility of the authors and does not necessarily represent the official views of the National Institutes of Health.

[1] Supported by National Institutes of Health Grants T32 GM007205 and F30 DK115037.

[2] Supported by National Institutes of Health Grants T32 GM007205 and F30 DK104596.

[3] To whom correspondence should be addressed: Section of Endocrinology and Metabolism, Dept. of Internal Medicine, Yale University School of Medicine, P. O. Box 208020, New Haven, CT 06520-8020. Tel.: 203-785-6319; Fax: 203-785-6462; E-mail: jonathan.bogan@yale.edu.

[4] The abbreviations used are: GSV, GLUT4 storage vesicle; HFD, high-fat diet; HFS, high-fat and sucrose diet; IRAP, insulin-regulated aminopeptidase; PI3K, phosphatidylinositol 3-kinase; Q-PCR, quantitative RT-PCR; RC, regular chow; TUG, tether containing a UBX domain for GLUT4; TUGUL, TUG ubiquitin-like; bis-tris, 2-[bis(2-hydroxyethyl)amino]-2-(hydroxymethyl) propane-1,3-diol; PM, plasma membrane; LM, light microsome; HM, heavy microsome; M/N, mitochondria/nuclei; nW, nanowatt; GWAT, gonadal white adipose tissue; TfR, transferrin receptor; DMEM, Dulbecco's modified Eagle's medium.

eter, and physicochemical characteristics of GSVs (8, 9). In 3T3-L1 adipocytes and *in vivo* in skeletal muscle, similar increases in glucose uptake are observed after TUG disruption and after maximal insulin stimulation; there is little or no further effect of insulin in cells with disrupted TUG action (7, 10). In muscle, the mobilization of TUG-bound vesicles results in IRAP translocation, so that glucose uptake is coordinated with inactivation of vasopressin, an IRAP substrate (11). TUG itself is a target of SIRT2-mediated deacetylation, which controls the size of the GSV pool and, consequently, insulin sensitivity (12). Thus, the TUG protein is a critical regulator of GSV accumulation and release and is a major site of insulin action.

To mobilize GSVs, insulin stimulates TUG cleavage. Intact TUG links GSVs to the Golgi matrix by binding GLUT4 and IRAP through its N terminus and Golgin-160 and other matrix proteins through its C terminus (7, 11–13). Insulin-triggered TUG cleavage separates these N- and C-terminal regions and is required for highly insulin-responsive GLUT4 translocation and glucose uptake (12, 13). Like the formation of an insulin-responsive pool of GSVs, TUG cleavage occurs in fat and muscle cells but is not observed in other cell types. Insulin-stimulated proteolytic processing of intact TUG produces a novel ubiquitin-like protein modifier, TUGUL (for TUG Ubiquitin-Like), but the major target of TUGUL modification ("tugulation") has not been identified (13). The TUG proteolytic pathway is thought to act in parallel to insulin signals transduced through phosphatidylinositol 3-kinase (PI3K), Akt, AS160/Tbc1D4, and target Rab proteins, which coordinate overall GLUT4 trafficking (9, 14, 15). It is not known whether attenuated TUG signaling may contribute to insulin resistance, independently of Akt (16). More broadly, how these insulin signaling and vesicle trafficking processes intersect remains to be fully elucidated. Here, we present data to support a model in which the TUG protease is Usp25m, and TUGUL modifies KIF5B (KIF5B, kinesin family member 5B) to load GSVs onto these kinesin motors.

Results

Previous results support the idea that intact TUG undergoes proteolytic processing, as diagrammed in Fig. 1*A*, to produce a ubiquitin-like modifier, TUGUL (13). Therefore, we considered that a deubiquitylating enzyme family member may act as the TUG protease. Among these enzymes, Usp25 (ubiquitin C-terminal hydrolase 25) was of particular interest because it was identified in a screen for proteins that bind tankyrase, an IRAP partner that regulates GLUT4 trafficking (17–21). In addition, Usp25 is present in distinct splice variants, including a muscle isoform that might account, at least in part, for the cell-type specificity of TUG cleavage in myocytes and adipocytes (22, 23). This muscle isoform, Usp25m, has additional exons encoding 70 residues not present in the ubiquitous isoform, Usp25a, so that it has a greater relative mass (24). These residues are internal, and how they contribute to the structure and function of Usp25m is not understood.

To learn whether a Usp25 protein is present in adipocytes, we used 3T3-L1 cells. These cells can be induced to undergo adipose tissue differentiation over the course of 8 days, and they are widely used for studies of GLUT4 translocation. As shown in Fig. 1*B*, immunoblots revealed that a Usp25 protein is induced early during adipocyte differentiation, so that its abundance is maximal by day 4. Data below indicate that this is the Usp25m isoform. Usp25m up-regulation coincided with the appearance of TUG cleavage products, which are present at 42 and 54 kDa (for the C-terminal product) and 130 kDa (for the N-terminal product, containing TUGUL attached to its major target protein), as described previously (13). To characterize what splice form of Usp25 is expressed in adipose tissue, we immunoblotted lysates prepared from mouse gonadal white adipose tissue (GWAT), quadriceps, other hindlimb muscles, and brain. As shown in Fig. 1*C*, the Usp25 protein in adipose tissue was observed at the same molecular mass as the Usp25m isoform present in skeletal muscles (predicted to be 130 kDa) and was clearly distinct from the smaller Usp25a isoform present in brain (predicted to be 122 kDa). These data support the idea that Usp25m is expressed in adipose, as well as in muscle cells. Possibly, Usp25m may function in GLUT4 regulation in both cell types. Here, we focus on its role in adipocytes.

To determine whether Usp25m interacts with TUG, we first performed coimmunoprecipitation experiments using transfected cells. Fig. 1*D* shows that TUG can be copurified with Usp25m, but substantially less well with Usp25a, when these proteins are coexpressed. On dark exposures of films from this experiment, we observed the TUG 42-kDa C-terminal cleavage product in lysates of cells transfected with Usp25m, but not Usp25a, as explored further below. To examine whether the endogenous Usp25m protein in 3T3-L1 adipocytes associates with TUG, we used a TUG protein containing a C-terminal biotin tag, as described previously (11). This protein is expressed using a retrovirus and is present at only slightly increased abundance compared with endogenous TUG protein in 3T3-L1 adipocytes. We purified TUG-bound vesicles from cell homogenates by incubation with immobilized streptavidin and analyzed the eluted proteins on immunoblots. Fig. 1*E* shows that Usp25m was copurified with TUG and that insulin stimulated its dissociation from TUG isolated using the C-terminal tag. Similar results were obtained for GLUT4, IRAP, VAMP2, LRP1, and VAMP3, which are all present in GSVs (25). Because the purification was done using immobilized streptavidin, we immunoblotted an endogenous biotinylated protein, acetyl-CoA-carboxylase, as a control. As predicted, the purification of this protein was unaffected by brief insulin stimulation. Previous data imply that AS160/TbC1D4, an Akt substrate through which insulin activates specific Rab GTPases, is also present on GSVs (26). We therefore repeated the experiment shown in Fig. 1*E* and immunoblotted AS160. As shown in Fig. 1*F*, AS160 was present on TUG-bound vesicles in unstimulated cells, and its abundance was greatly reduced by prior insulin stimulation, similar to results obtained for other GSV proteins. Together, the data support the idea that Usp25m associates with TUG-bound GSVs in unstimulated 3T3-L1 adipocytes and that insulin stimulates the acute mobilization of Usp25m, as well as these vesicles, from the TUG C terminus.

We also tested whether Usp25m associates with GLUT4 itself. We used 3T3-L1 adipocytes that stably express a GLUT4 reporter protein, GLUT4–7myc-GFP, described previously

(27), and prepared lysates using nonionic detergent. As shown in Fig. 1*G*, endogenous Usp25m coimmunoprecipitated with this GLUT4 protein in unstimulated cells. In repeated experiments, about a third of these complexes were disassembled after insulin stimulation (32 ± 7%, mean ± S.E., $p < 0.01$, $n = 4$). Previous data show that two-thirds of intact TUG proteins are similarly released from GLUT4 after insulin stimulation (6). Together, the data support the idea that Usp25m is expressed in

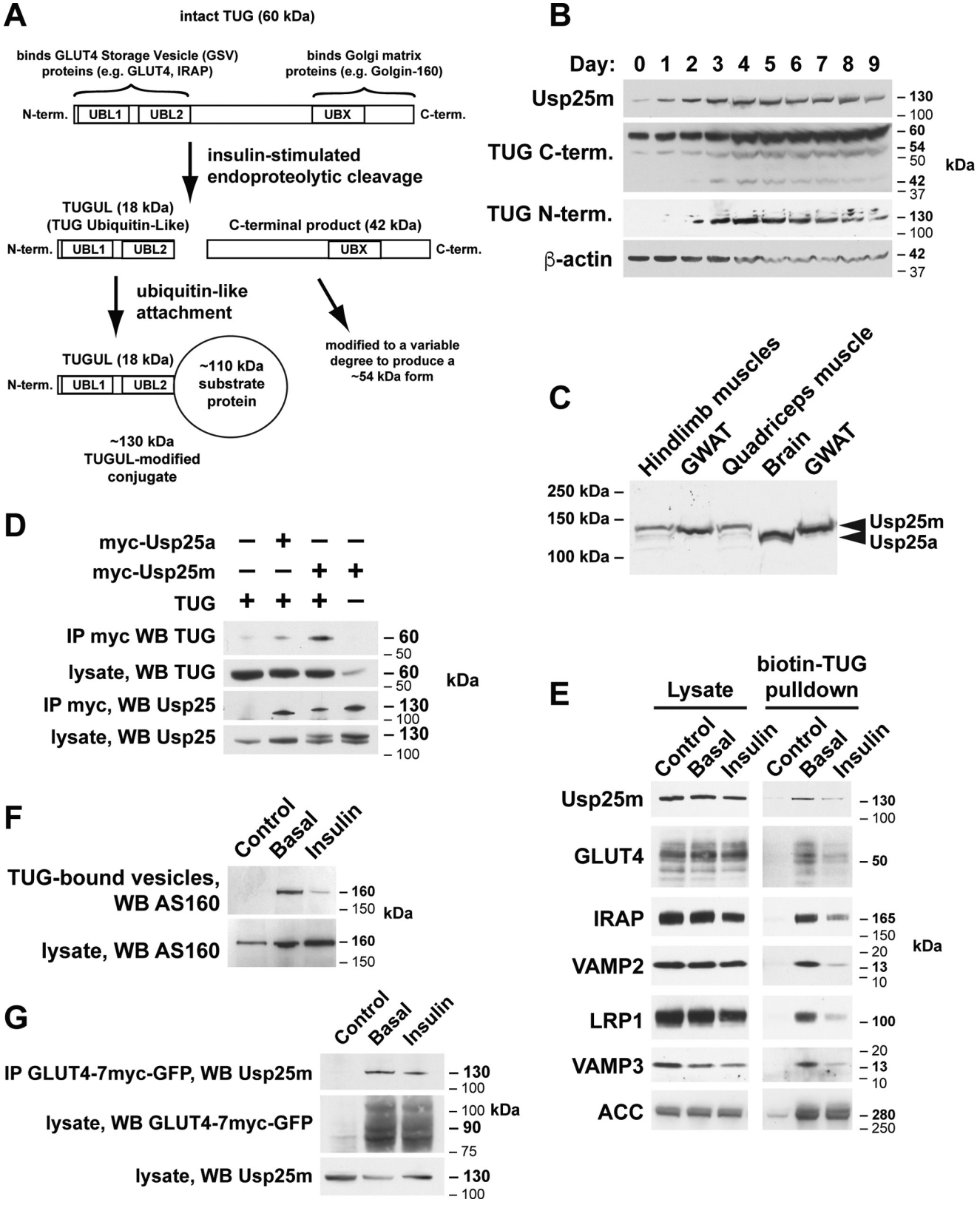

adipocytes and that it interacts with TUG and with insulin-responsive GLUT4.

To examine whether Usp25m colocalizes with GSVs, we performed subcellular fractionation experiments. We separated 3T3-L1 adipocytes into cytosol, plasma membrane (PM), light microsome (LM), heavy microsome (HM), and mitochondria/nuclei (M/N) fractions, as described previously (7, 27). The LM fraction contains GSVs and intact TUG (6, 7, 13). In Fig. 2*A*, immunoblotting confirmed that IRAP is mobilized out of the LM fraction and to the PM after brief insulin stimulation. Usp25m was present in the LM fraction and was not abundant in other fractions in unstimulated cells. Insulin stimulated the mobilization of Usp25m from the LM fraction into the cytosol. These data are consistent with data in Fig. 1, which imply that Usp25m binds GLUT4 and TUG proteins present on GSVs and dissociates from these vesicles after insulin stimulation.

In preliminary studies, we observed the 42-kDa TUG C-terminal cleavage product on membranes with characteristics of lipid rafts. We considered that if the product is generated on these membranes, then at least some Usp25m proteins may partition in raft fractions. Accordingly, we used a flotation assay to separate raft and nonraft membranes from basal and insulin-stimulated 3T3-L1 adipocytes. As shown in Fig. 2*B*, rafts containing caveolin were present in fractions 2–7, whereas nonraft membranes were present in fractions 8–12. A subset of the raft fractions contained flotillin. Intact TUG and Usp25m were present in similar distributions spanning raft and nonraft fractions and were slightly redistributed to rafts in insulin-stimulated cells. Whereas the 42-kDa TUG product was observed only in nonraft fractions in unstimulated cells, this product was present in raft fractions of insulin-stimulated cells. The TUG C-terminal antibody detected additional bands at ~46 and at 25 kDa, which may represent other TUG-derived products. The 54-kDa modified TUG C-terminal product observed previously (13) was present almost exclusively in nonraft fractions. Together with other results, the data support the idea that Usp25m activity generates the 42-kDa TUG C-terminal cleavage product on membranes with characteristics of lipid rafts.

We also studied whether Usp25m colocalizes with GLUT4 using confocal microscopy of 3T3-L1 adipocytes containing the GFP-tagged GLUT4 reporter protein. We observed intracellular punctae at which Usp25m and GLUT4 colocalized in the basal (unstimulated) state (Fig. 2*C*). After insulin stimulation, GLUT4 was observed at the plasma membrane, and there seemed to be fewer intracellular punctae containing colocalized Usp25m. We conclude that Usp25m binds and colocalizes with insulin-responsive GSVs and that it dissociates from these membranes after insulin stimulation.

We used shRNAs to study whether Usp25m is required for insulin-stimulated TUG proteolysis. We expressed these shRNAs in 3T3-L1 adipocytes using retroviruses. Initial testing of five different shRNAs showed that four effectively depleted Usp25m, as shown in Fig. 3*A*. Immunoblots using an antibody to the TUG C terminus showed that the ratio of the C-terminal product to intact TUG was markedly reduced in cells in which Usp25m was depleted, supporting the idea that Usp25m is required for TUG cleavage. To examine more closely whether Usp25m knockdown blocks insulin action, we used control 3T3-L1 adipocytes and cells containing shRNAs #1 and #3, which most effectively depleted Usp25m. We treated these cells for 30 min using a range of insulin concentrations, as shown in Fig. 3*B*. Insulin caused a concentration-dependent increase in the abundance of the TUG C-terminal product in control 3T3-L1 adipocytes. Usp25m knockdown abrogated the ability of insulin to stimulate the generation of this product. This result was observed using both shRNAs, supporting the idea that it is not an off-target effect and that Usp25m is required for TUG cleavage. In addition, we studied insulin signaling through Akt, using an antibody to immunoblot Akt phospho-Ser-473. Usp25m knockdown had no effect on insulin-stimulated Akt phosphorylation. This observation is consistent with previous data, which show that TUG cleavage requires the GTPase TC10α, and that the TC10α effector PIST binds TUG and transduces an insulin signal to regulate TUG cleavage (10, 13). Quantification of the TUG product and phospho-Akt in Fig. 3*B* further showed that these two pathways have different insulin sensitivities. The phospho-Akt response was half-maximal at 1.3 nM insulin and reached an essentially maximal response at 6.4 nM insulin. The TUG cleavage response was half-maximal at 6.4 nM insulin and reached a maximal response at 32 nM insulin. Thus, under these experimental conditions, these two insulin responses have distinct sensitivities, with the phospho-Akt response as the more sensitive insulin signal.

To show more definitively that insulin-stimulated TUG cleavage and Akt phosphorylation are independent of each other, we used control and Usp25 shRNA#1 3T3-L1 adipocytes treated in the absence or presence of wortmannin, a PI3K inhibitor. As shown in Fig. 3*C*, insulin stimulated the production of the N- and C-terminal TUG products in control cells. The N-terminal TUG product, TUGUL, was incorporated into a 130-kDa protein, and the C-terminal product was present in 42- and 54-kDa forms, as described previously (13). The gener-

Figure 1. Usp25m is present in adipocytes and binds TUG and GLUT4. *A,* diagram of TUG processing is shown, based on previous data. Insulin stimulates cleavage of the 60-kDa intact protein to generate 18-kDa N-terminal and 42-kDa C-terminal products. The N-terminal product, TUGUL, is covalently attached to a substrate protein to make a 130-kDa conjugate. The C-terminal product is modified to a variable extent to make an ~54-kDa form. *B,* 3T3-L1 cells were lysed at the indicated days after induction of adipocyte differentiation. Lysates were immunoblotted to detect the indicated proteins, including Usp25, intact TUG (60 kDa), TUG C-terminal products (54 and 42 kDa), and TUG N-terminal products (130 kDa). *C,* lysates prepared from the indicated mouse tissues were analyzed by SDS-PAGE and immunoblotting using a Usp25 antibody, which distinguished the Usp25a and Usp25m splice forms. *D,* Myc-tagged Usp25a and Usp25m proteins expressed together with TUG in transfected 293 cells. Immunoprecipitations (*IP*) were performed using anti-Myc antibody, and immunoblots (*WB*) of eluted proteins and of the lysates were done as indicated. *E,* TUG containing a C-terminal biotin tag was stably expressed in 3T3-L1 adipocytes. Vesicles were then purified from homogenates of basal and insulin-stimulated cells using immobilized neutravidin (pulldown). As a negative control, biotin-saturated neutravidin was used. Eluted proteins and control lysates were immunoblotted to detect the indicated proteins. Acetyl-CoA carboxylase (*ACC*) is an endogenous biotinylated protein that was used as a positive control for the purification. *F,* TUG-containing vesicles were purified as in *D* and were immunoblotted to detect AS160/Tbc1D4. *G,* anti-GFP antibody was used to immunoprecipitate GLUT4–7myc-GFP from lysates of 3T3-L1 adipocytes stably expressing this GLUT4 reporter protein, and in lysates of control cells not expressing this protein. Eluates and lysates were immunoblotted as indicated.

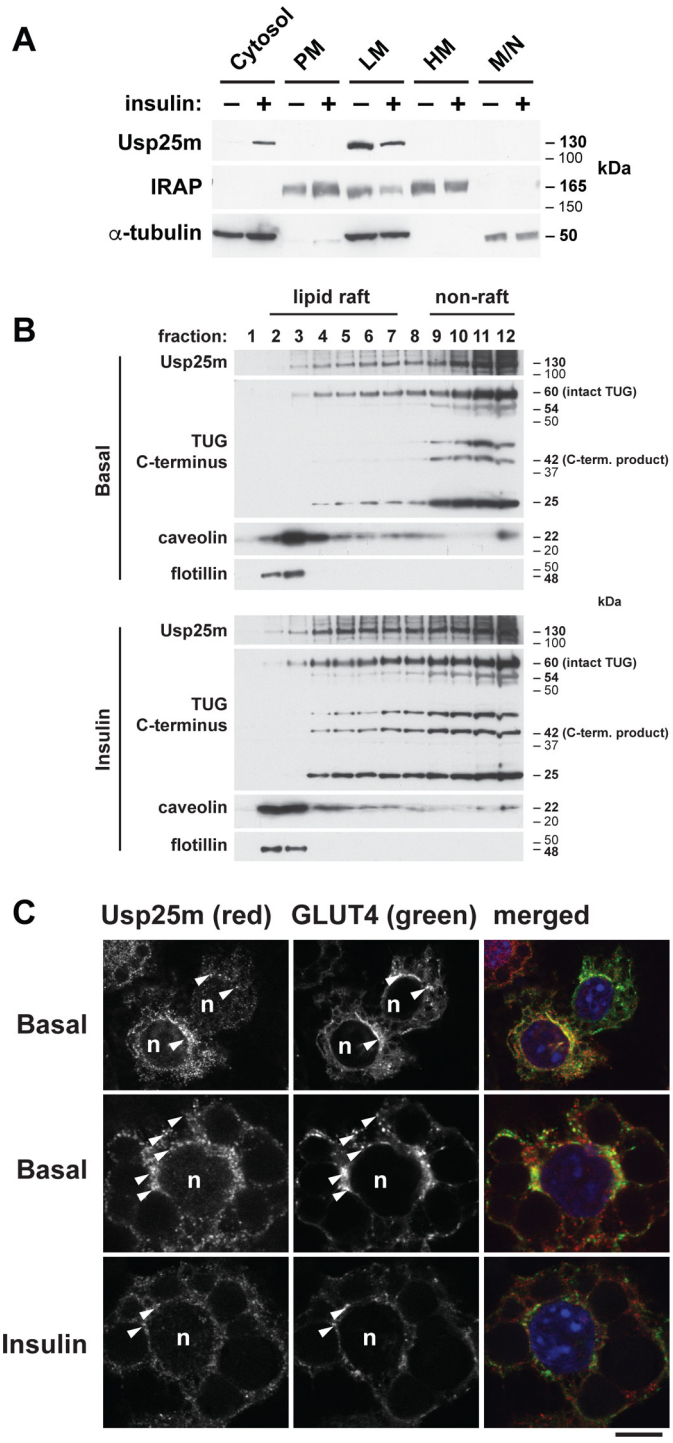

Figure 2. Usp25m colocalizes with TUG and with proteins in insulin-responsive vesicles. *A,* basal and insulin-stimulated 3T3-L1 adipocytes were subjected to subcellular fractionation. The indicated fractions were immunoblotted to detect Usp25m and IRAP proteins. *B,* lipid raft and nonraft membrane fractions were isolated from basal, unstimulated 3T3-L1 adipocytes and from cells stimulated acutely (8 min) with insulin. Fractions were immunoblotted as indicated. *C,* basal and insulin-stimulated 3T3-L1 adipocytes were imaged using confocal microscopy. GLUT4 reporter was detected using the GFP tag, and Usp25m was detected by immunostaining. *Arrowheads* indicate colocalized punctae. *n* indicates nucleus. *Scale bar,* 10 μm.

ation of these products was unaffected by wortmannin pretreatment of the cells. As a positive control, immunoblotting of Akt phospho-Ser-473 showed that wortmannin blocked insulin-stimulated Akt phosphorylation. Thus, insulin-stimulated TUG cleavage does not require signaling through PI3K. By contrast, Usp25m knockdown blocked the ability of insulin to stimulate production of the TUG N- and C-terminal cleavage products. Usp25m depletion did not affect insulin-stimulated Akt phosphorylation, similar to results obtained in Fig. 3*B*. Finally, in cells containing the Usp25m shRNA and also treated with wortmannin, neither TUG products nor Akt phosphorylation was observed after insulin stimulation. The data show that insulin acts through two independent signaling pathways in adipocytes, one that requires PI3K activity and results in Akt phosphorylation, and another that requires Usp25m and results in TUG proteolytic cleavage.

Our data predicted that the translocation of GSV cargoes, including GLUT4, would be impaired by Usp25m knockdown. Therefore, we assessed insulin-stimulated translocation in 3T3-L1 adipocytes containing the Usp25 shRNAs, compared with control cells. We first used cells stably expressing the GLUT4–7myc-GFP reporter and imaged the surface-exposed Myc epitope tag, as well as GFP (12, 13). As shown in Fig. 4*A*, insulin stimulated a dramatic increase in GLUT4 at the surface of control cells and had no large effect on total abundance of the tagged GLUT4 reporter. This effect was completely inhibited in Usp25 shRNA#1 cells, supporting the idea that Usp25m is required for insulin-stimulated GLUT4 translocation. Data were quantified in Fig. 4*B*, which plots the ratio of Myc- to GFP-fluorescence intensities for several cells in each group and which includes data for Usp25 shRNA#3 cells. As can be seen, insulin stimulated an ~12-fold increase in surface to total GLUT4 in control cells, and this effect was blocked by both Usp25 shRNAs. The data support the idea that Usp25m is required for insulin-stimulated GLUT4 translocation. This conclusion is consistent with observations, above, that Usp25m is required for TUG cleavage, and with previous work showing that TUG cleavage is required for GLUT4 translocation (13).

To further test whether Usp25m knockdown impairs insulin-stimulated translocation of GLUT4 and IRAP, we biotinylated surface-exposed proteins in basal and insulin-stimulated 3T3-L1 adipocytes. Fig. 4*C* shows that although insulin stimulated the translocation of both GLUT4 and IRAP to the plasma membrane in control cells, translocation was not observed in Usp25 shRNA#1 and shRNA#3 cells. Of note, total GLUT4 abundance was reduced by Usp25m knockdown, and there was no large change in total IRAP abundance. Although GLUT4 abundance is reduced by knockdown of the GSV-budding protein sortilin (28), we observed no decrease in sortilin abundance in Usp25m knockdown cells, as shown in Fig. 4*D*. Insulin had no large effect on the cell-surface transferrin receptor (TfR) in control cells, consistent with the idea that TfR is not abundant in GSVs (25, 26). Data from several cell-surface biotinylation experiments are quantified in Fig. 4*E*. These data show that Usp25m knockdown completely blocked the ability of insulin to stimulate translocation of GLUT4 and IRAP. For TfR, translocation was not observed in control cells or in cells with Usp25m depletion. For each protein, the data are expressed as the fold-translocation stimulated by insulin, which is the ratio of the plasma membrane abundance in insulin-stimulated cells to that in unstimulated cells. Together, the data support the

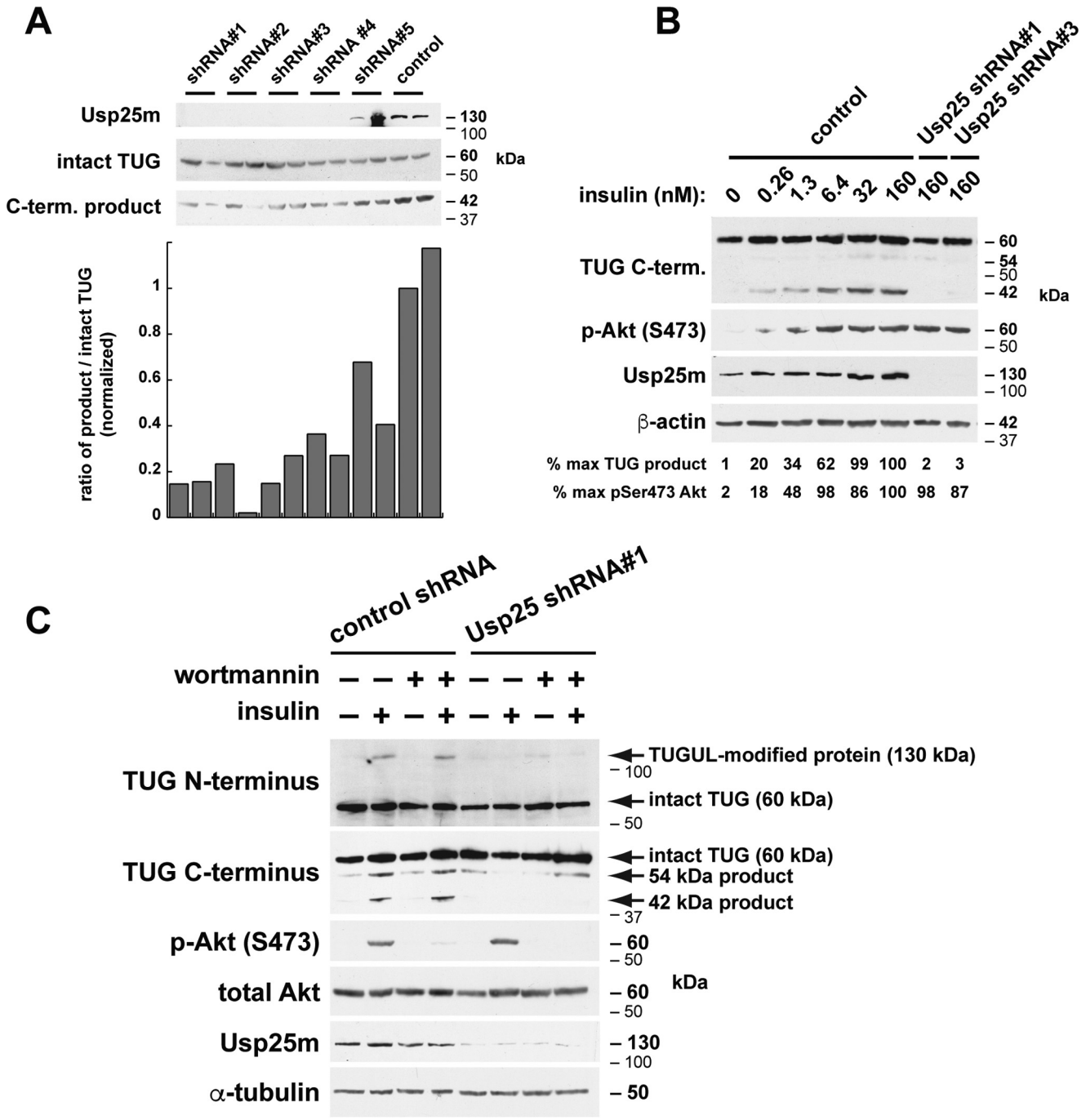

Figure 3. TUG endoproteolytic cleavage requires Usp25m and is insensitive to wortmannin. *A,* retroviruses were used to express five different shRNAs targeting Usp25m, or a control nontargeting shRNA, in 3T3-L1 adipocytes. Cells were lysed and immunoblotted as indicated. *B,* control 3T3-L1 adipocytes and cells expressing Usp25 shRNAs were treated with the indicated concentrations of insulin for 30 min. Cells were then lysed and immunoblotted to detect intact TUG and the C-terminal proteolytic product, phospho-Akt, and Usp25m, as indicated. *C,* control and Usp25 shRNA 3T3-L1 adipocytes were treated with wortmannin (100 nM) for 45 min as indicated, and insulin (160 nM) was added for the last 30 min of this period as indicated. Cells were lysed, and immunoblots were performed using the indicated antibodies.

idea that Usp25m is required not only for TUG cleavage but also for the specific mobilization of GSV cargo proteins to the cell surface in 3T3-L1 adipocytes.

We next sought to identify the target that is covalently modified by attachment of TUGUL, the TUG N-terminal cleavage product. Previous data show that insulin stimulates the microtubule-based movement of GLUT4 and that this is mediated by KIF5B, a 110-kDa kinesin motor that is markedly up-regulated during 3T3-L1 adipocyte differentiation (29). TUGUL contains two tandem ubiquitin-like domains (13, 30). Its mass will contribute 18 kDa to the total ~130-kDa mass of the modified (*i.e.* tugulated) target substrate in 3T3-L1 adipocytes (if one TUGUL is used for the modification). This implies that the target of modification is ~110 kDa, consistent with the relative mass of KIF5B. More importantly, insulin stimulates both KIF5B-mediated GLUT4 movement and insulin-stimulated

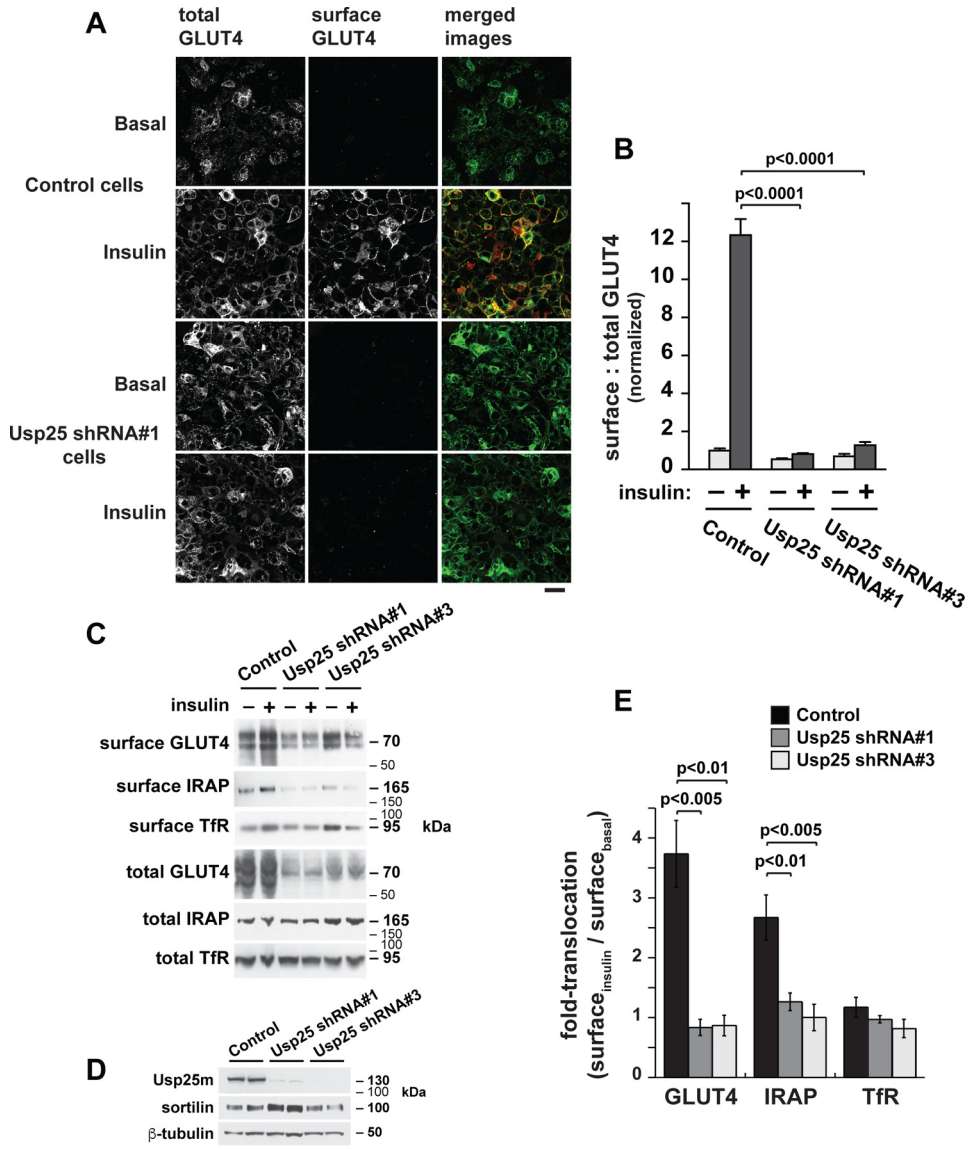

Figure 4. Usp25m knockdown inhibits insulin-stimulated GLUT4 and IRAP translocation. *A* and *B,* 3T3-L1 adipocytes containing control or Usp25-targeting shRNAs, and expressing the GLUT4–7myc-GFP reporter, were left unstimulated or treated with insulin, as indicated. Using unpermeabilized cells, externalized Myc tag (surface GLUT4) and GFP (total GLUT4) were imaged using confocal microscopy. *A,* representative images of fields of cells are shown. *Scale bar,* 40 μm. *B,* ratios of surface to total fluorescence intensities were quantified for several cells under each condition (n = 17–27 in each group). *C,* control and Usp25 shRNA-containing 3T3-L1 adipocytes expressing the GLUT4 reporter protein were stimulated with insulin, as indicated, and then cell-surface proteins were biotinylated at 4 °C. Surface-exposed proteins were purified using immobilized neutravidin, and eluates and whole-cell lysates were immunoblotted as indicated to detect GLUT4, IRAP, and TfR. *D,* cell-surface biotinylation experiments were used to assess insulin-stimulated translocation of GLUT4, IRAP, and TfR in control 3T3-L1 adipocytes and cells containing Usp25 shRNAs, as indicated. (n = 3–5 in each group). Data were quantified and are plotted. *E,* whole-cell lysates of control 3T3-L1 adipocytes and cells containing Usp25 shRNAs were immunoblotted to detect Usp25m and sortilin, as indicated.

TUGUL modification in a wortmannin-insensitive manner (Fig. 3*C*) (29). Finally, KIF5B carries GLUT4 from the perinuclear region to the cell periphery, which might reasonably be coupled to release of the GSVs from the Golgi matrix.

To study whether KIF5B is a target of TUGUL modification, we used several approaches. First, we immunoblotted primary and 3T3-L1 adipocytes to show that upon insulin stimulation, KIF5B is modified to produce an SDS-resistant ~130-kDa form, consistent with the attachment of TUGUL. To study primary adipocytes, we treated mice by intraperitoneal injection of insulin/glucose solution or saline control. We sacrificed the mice after 30 min, isolated GWAT, and prepared and immunoblotted lysates using antibodies to KIF5B and the TUG N terminus. As shown in Fig. 5*A*, we observed KIF5B bands at both 110 kDa (corresponding to unmodified KIF5B) and at 130 kDa (the predicted mass of tugulated KIF5B). The abundance of the 130-kDa KIF5B protein was increased dramatically after insulin stimulation, so that it accounted for about half of the total KIF5B detected in the lysates. On immunoblots using an antibody to the TUG N terminus, both intact TUG (60 kDa) and the TUGUL-modified protein (130 kDa) were observed. Insulin caused a decrease in the abundance of intact TUG, as quantified further below, together with a dramatic increase in the abundance of the TUGUL-modified 130-kDa protein. Similar results were obtained in 3T3-L1 adipocytes, as shown in Fig. 5*B*. In 3T3-L1 cells, the effect of insulin was often not as dramatic as

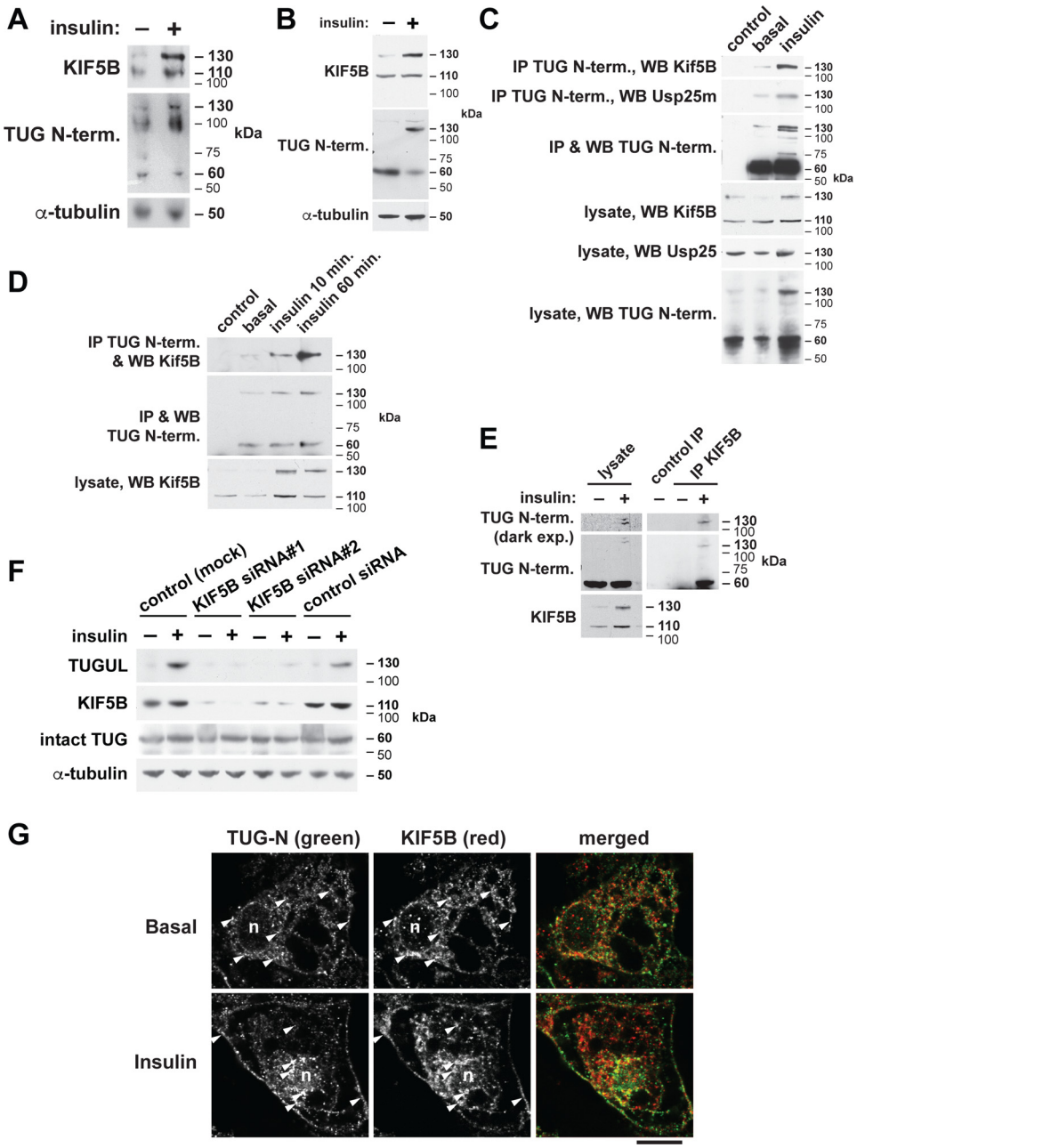

Figure 5. Insulin stimulates TUGUL modification of KIF5B. *A,* mice were treated by intraperitoneal injection of insulin/glucose solution, or saline control, and sacrificed 30 min later. Gonadal white adipose tissue was isolated, lysed, and immunoblotted to detect KIF5B and the TUG N terminus, as indicated. *B,* 3T3-L1 adipocytes were treated with insulin (160 nm, 30 min) as indicated, then lysed, and immunoblotted to detect KIF5B and the TUG N terminus. *C,* 3T3-L1 adipocytes were treated with insulin (160 nm, 30 min) as indicated, and then the endogenous TUG N terminus was immunoprecipitated. Immunoblots were done to detect KIF5B, TUG N terminus, and Usp25m, as indicated. *D,* 3T3-L1 adipocytes were treated with insulin for the indicated lengths of time and then lysed using denaturing conditions. Lysates were diluted in nonionic detergent, and then the endogenous TUG N terminus was immunoprecipitated. Immunoblots were performed as indicated. *E,* 3T3-L1 adipocytes were treated with insulin as indicated, and then the endogenous KIF5B protein was immunoprecipitated. Immunoblots were performed to detect KIF5B and TUG N-terminal products. *F,* 3T3-L1 adipocytes were transfected with siRNAs targeting KIF5B, as indicated. Two days later, cells were treated with or without insulin and then lysed and immunoblotted as indicated. *G,* basal and insulin-stimulated 3T3-L1 adipocytes were imaged using immunofluorescence confocal microscopy to detect the TUG N terminus and KIF5B. *Arrowheads* indicate colocalized punctae. *N* indicates nucleus. *Scale bar,* 10 μm.

was observed in primary adipocytes. Nonetheless, in well-differentiated cells, KIF5B modification was observed and appeared concurrently with the TUGUL-modified protein at the same relative mass. These data are consistent with the idea that TUGUL modifies KIF5B.

To further test whether TUGUL is attached to KIF5B, we performed immunoprecipitations using 3T3-L1 adipocytes and an antibody to the TUG N terminus, and we immunoblotted the eluates to detect KIF5B. In Fig. 5*C*, this was done under nondenaturing conditions, and both KIF5B and Usp25m were copurified with the TUG N terminus in insulin-stimulated cells. The tugulated substrate and KIF5B were similarly increased in abundance after insulin stimulation, as was the copurified Usp25m. To support the idea that the TUGUL–

KIF5B association is covalent, we also performed immunoprecipitations after denaturing lysis of 3T3-L1 adipocytes. In these experiments, SDS was neutralized with nonionic detergent prior to addition of the immunoprecipitating antibody. As shown in Fig. 5*D*, KIF5B was again coimmunoprecipitated with the TUGUL-modified protein. The abundances of both proteins increased progressively in cells treated with insulin for a longer duration. We also performed the converse immunoprecipitation in Fig. 5*E*. Here, KIF5B was immunoprecipitated from basal and insulin-stimulated 3T3-L1 cells, and the tugulated protein was copurified in the insulin-stimulated cells. These data support the hypothesis that upon insulin stimulation, TUGUL modifies KIF5B in 3T3-L1 adipocytes.

To further test the idea that KIF5B is the target of TUGUL modification, we used RNAi to knock down KIF5B in 3T3-L1 adipocytes. Two different siRNA duplexes targeting KIF5B were transfected into differentiated adipocytes. Basal and insulin-stimulated cells were then lysed and immunoblotted. As shown in Fig. 5*E*, KIF5B was effectively depleted in cells treated with the siRNAs. In this experiment, the H2 mAb used for KIF5B detected the 110-kDa unmodified kinesin and was less sensitive for the 130-kDa modified form (see "Experimental procedures"). Whereas insulin stimulated the TUGUL modification of a substrate protein in control cells, the production of this TUGUL-modified protein was dramatically absent in the KIF5B-depleted cells. Thus, data from both copurification and RNAi-mediated knockdown support the concept that TUGUL modifies KIF5B. Taken together with previous results, we conclude that KIF5B is the major target of TUGUL modification in 3T3-L1 adipocytes.

If TUG cleavage not only liberates GSVs from the Golgi matrix, but also initiates the microtubule-based movement of these vesicles to the cell periphery, then the TUG N terminus may be relocated after insulin stimulation. Previous data show that the TUGUL-modified substrate is present in plasma membrane fractions of 3T3-L1 adipocytes, consistent with this idea (13). To further test whether KIF5B and TUGUL are colocalized at a peripheral location after insulin treatment, we used confocal microscopy. Fig. 5*F* shows that KIF5B and TUGUL colocalize, at least to some degree, in unstimulated 3T3-L1 adipocytes. After insulin stimulation, both proteins are more prominent near the plasma membrane, and colocalization is maintained, consistent with previous results for KIF5B (29). The images also show that a substantial fraction of the KIF5B does not colocalize with TUGUL, consistent with the idea that a fraction of KIF5B proteins are modified in 3T3-L1 adipocytes. We conclude that insulin stimulates the action of Usp25m to catalyze TUG cleavage and that the liberated N-terminal product, TUGUL, is attached to KIF5B, a kinesin motor previously reported to carry GLUT4 to the plasma membrane.

TUGUL binds noncovalently to GLUT4 and IRAP (7, 11), implying that its covalent attachment to KIF5B may load GSVs on to these kinesin motors. We therefore considered whether insulin stimulates the association of GLUT4 with KIF5B and whether TUG proteolytic processing is required for this association. To test these ideas, we immunoprecipitated the GFP-tagged GLUT4 reporter from control and Usp25m-depleted cells, and we immunoblotted KIF5B. As shown in Fig. 6*A*, insulin treatment caused the association of KIF5B with GLUT4 in WT cells, and this effect was ablated in cells containing the Usp25 shRNAs. These data support the idea that Usp25m acts through TUG proteolysis to stimulate the insulin-stimulated association of GLUT4 with KIF5B.

To further show that binding of GLUT4 to KIF5B requires TUG proteolytic processing, we used 3T3-L1 adipocytes containing cleavage-defective mutated forms of TUG. We previously showed that changing the two glycine residues at the TUG cleavage site to alanine residues resulted in a cleavage-resistant form of TUG, TUG GGAA, that did not support GLUT4 translocation in shRNA rescue experiments (13). Data suggested that this TUG GGAA protein was cleavage-resistant but not absolutely cleavage-defective. Therefore, to create a more effective cleavage-deficient mutant, we changed these glycine residues to valines, based on precedents for ubiquitin (31, 32). As the catalytic cleft of thiol-type deubiquitylating enzymes can be quite narrow (33), we also mutated the glycines to tyrosine residues, which we hypothesized might be too bulky to interact at the catalytic site. The resulting proteins, TUG GGVV and TUG GGYY, were stably expressed at ~6-fold the abundance of endogenous TUG in 3T3-L1 adipocytes, using retrovirus vectors. As shown in Fig. 6*B*, insulin stimulated the interaction of GLUT4 with KIF5B in cells containing WT TUG but not in cells containing TUG GGVV or TUG GGYY. Intact TUG dissociated from GLUT4 after insulin stimulation of cells containing WT TUG, but not TUG GGVV or GGYY, as would be predicted if dissociation results from TUG cleavage. Control experiments support the idea that TUG GGVV and TUG GGYY are indeed cleavage-deficient, because the TUG C-terminal cleavage product was produced after insulin stimulation in control cells but not in cells containing these mutated proteins (Fig. 6*C*). As a further control, cells containing TUG GGVV or TUG GGYY did not exhibit insulin-stimulated translocation of IRAP or GLUT4, as assessed using cell-surface biotinylation (Fig. 6*D*), confocal microscopy (Fig. 6*E*), and subcellular fractionation (Fig. 6*F*). Of note, the subcellular fractionation experiments in Fig. 6*F* were done using control cells that overexpressed WT TUG and further show that the distributions of WT and mutated TUG GGVV proteins are similar. These proteins are most abundant in the LM fraction, similar to endogenous TUG (7, 13, 27). Thus, consistent with previous data using TUG GGAA, the results show that TUG cleavage is impaired when the diglycine sequence is mutated and that this results in impaired GLUT4 and IRAP translocation. Furthermore, neither TUG GGVV nor TUG GGYY supports the transfer of GLUT4 onto KIF5B, demonstrating that TUG cleavage is required for this process. Together with other data, we conclude that Usp25m-mediated TUG processing is required for tugulation of KIF5B and for loading of GLUT4 onto this motor protein in response to insulin.

To study whether expression of Usp25m and other proteins can reconstitute TUG proteolysis in noninsulin-responsive cells, we transfected HEK293 cells. GSV-like vesicles are not present in these cells, and we hypothesized that proteins present on GSVs form a complex that is required to support TUG proteolysis. Therefore, we expressed Usp25m alone or together with proteins known to be present on GSVs. Fig. 7*A* shows that

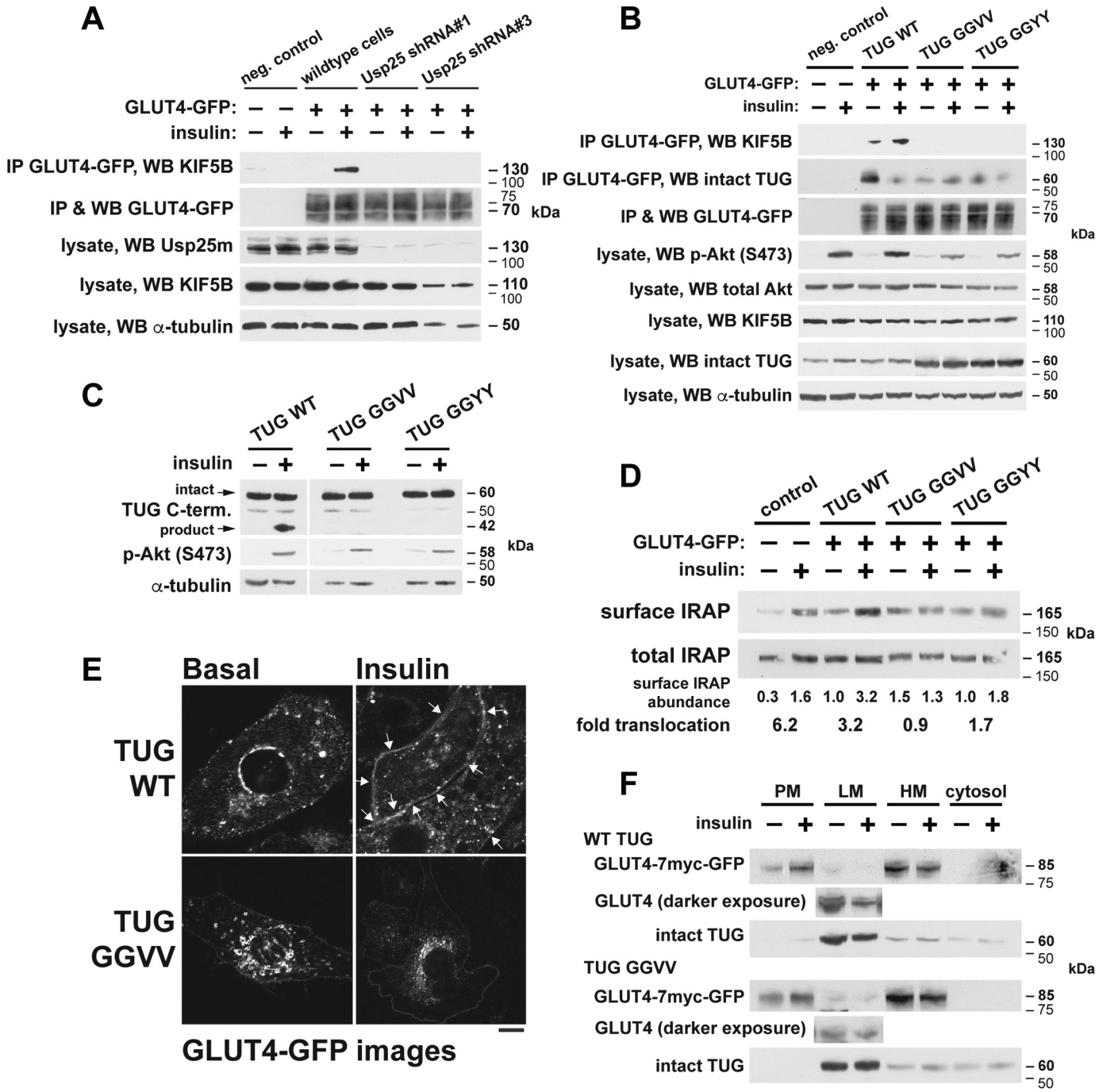

Figure 6. TUG proteolytic processing is required for insulin-stimulated association of GLUT4 with KIF5B. *A,* 3T3-L1 adipocytes expressing the GFP-tagged GLUT4 reporter protein, with or without Usp25 shRNAs, were treated with insulin (160 nm, 30 min) as indicated. Cells were lysed, and GLUT4 was immunoprecipitated (*IP*) using the GFP tag. Eluates were immunoblotted to detect copurified KIF5B. *B,* 3T3-L1 adipocytes expressing the GFP-tagged GLUT4 reporter, and containing WT or mutated TUG proteins as indicated, were treated with insulin and used for immunoprecipitations as in *A*. Eluates were immunoblotted to detect copurified KIF5B. *C,* 3T3-L1 adipocytes containing WT or cleavage site-mutated TUG proteins, as indicated, were treated with insulin and immunoblotted to detect intact TUG and the C-terminal cleavage product. Control Western blottings (*WB*) were done with the indicated antibodies. *D,* cells were treated with insulin, as indicated, and cell-surface proteins were biotinylated at 4 °C. After lysis, surface-exposed proteins were purified using immobilized neutravidin, and eluates and whole-cell lysates were immunoblotted to detect IRAP. Densitometry was used to measure the relative abundance of cell-surface IRAP and to calculate the fold-increase after insulin treatment, as indicated. *E,* 3T3-L1 adipocytes expressing the GFP-tagged GLUT4 reporter, together with WT or mutated TUG proteins as indicated, were treated with insulin and then imaged using confocal microscopy. *Arrows* indicate GLUT4 at the plasma membrane. *Scale bar,* 5 μm. *F,* 3T3-L1 adipocytes containing the GLUT4 reporter and overexpressed WT TUG or TUG GGVV were subjected to subcellular fractionation. Immunoblots were done on the indicated fractions to detect GLUT4 reporter and intact TUG, using anti-Myc and anti-TUG C-terminal antibodies.

transfection of Usp25m alone had a minimal effect to cleave endogenous TUG proteins but that TUG cleavage was greatly enhanced by coexpression of the GSV-regulating proteins sortilin and AS160. GLUT4 was transfected in all cases and may also play a role to facilitate TUG cleavage. When sortilin and AS160 were both cotransfected with Usp25m, the ratio of C-terminal cleavage product to intact TUG was increased by nearly 10-fold. Although some cleavage was observed in cells

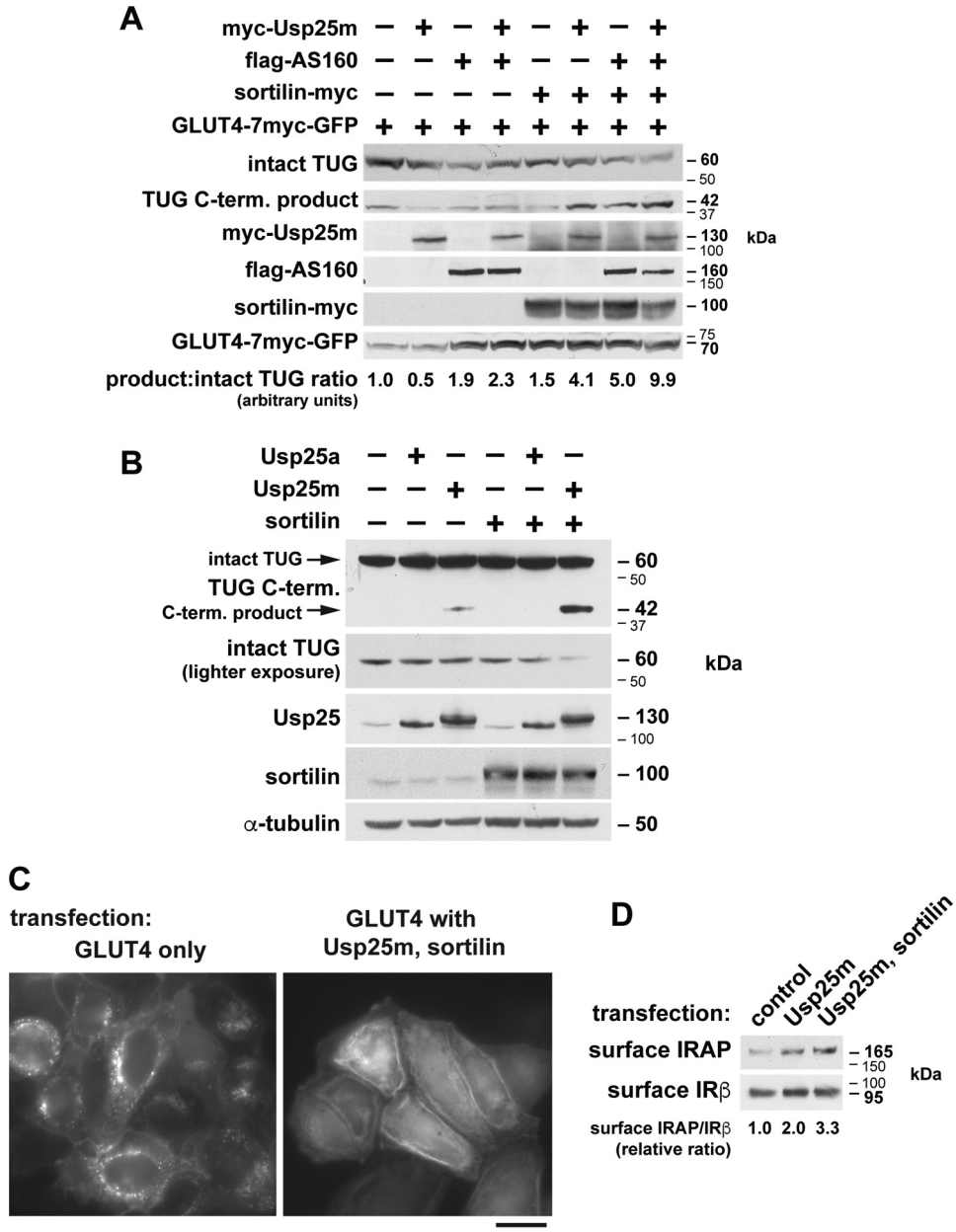

Figure 7. Reconstitution of TUG cleavage and GLUT4 and IRAP translocation in transfected cells. *A,* tagged Usp25m, sortilin, and AS160 proteins were expressed by transient transfection in 293 cells, as indicated. Immunoblots were done to detect endogenous intact TUG and its C-terminal cleavage product, as well as the transfected proteins. Abundances of intact TUG and the C-terminal product were measured by densitometry, and the relative ratio of product-to-intact TUG is shown. *B,* Usp25a, Usp25m, and sortilin proteins were overexpressed by transient transfection of HeLa cells, as indicated. GLUT4 reporter was also transfected using low amounts of plasmid in all samples. Immunoblots were performed to detect endogenous intact TUG and its C-terminal cleavage product, as well as the transfected proteins as indicated. *C,* HeLa cells were transfected with GLUT4 reporter alone or in combination with Usp25m and sortilin and were imaged by fluorescence microscopy of the GFP tag on GLUT4. *Scale bar,* 20 μm. *D,* HeLa cells were transfected as indicated, and cell-surface proteins were biotinylated and purified on immobilized neutravidin. Eluted proteins were immunoblotted to detect IRAP and, as a control, insulin receptor β-chain (*IR*β).

transfected with GLUT4, sortilin, and AS160 alone, overexpression of Usp25m invariably enhanced TUG proteolysis. We also examined the specificity of TUG proteolysis for Usp25m *versus* Usp25a. We transfected these proteins together with sortilin and reduced amounts of GLUT4, using 293 cells and HeLa cells. Similar results were obtained using both cell types, and data from HeLa cell transfections are shown in Fig. 7*B*. Immunoblots of endogenous TUG protein showed that the 42-kDa cleavage product was generated only when Usp25m was transfected and not by Usp25a. The abundance of this product was increased by cotransfection of sortilin, consistent with data in Fig. 7*A*. On a lighter exposure of the TUG immunoblot, depletion of intact TUG can be observed in the cells transfected with both Usp25m and sortilin. No effect of sortilin alone was observed. These data support the idea that Usp25m acts specifically to cleave TUG and that this effect is enhanced by coexpression of sortilin in nonadipocyte cells.

We next examined whether cotransfection of Usp25m, GLUT4, and sortilin is sufficient to redistribute GSV proteins in nonadipocyte cells. We transfected HeLa cells using the GFP-

tagged GLUT4 reporter, with or without Usp25m and sortilin. As shown in Fig. 7*C*, fluorescence microscopy showed that in control cells transfected with GLUT4 only, the GFP-tagged GLUT4 was present primarily in punctate structures arranged in a perinuclear pattern. In contrast, when the cells were cotransfected with Usp25m and sortilin, the GLUT4 was redistributed away from the nucleus and appeared to accumulate in the plasma membrane. To further test whether transfection of Usp25m and sortilin causes the translocation of GSV cargo proteins, we used biotinylation to assess the exposure of endogenous IRAP at the cell surface. Fig. 7*D* shows that transfection of HeLa cells with Usp25m alone, or with Usp25m and sortilin, caused a progressive increase in the plasma membrane abundance of IRAP. As a control, the abundance of insulin receptor β-chain observed at the cell surface was unaffected. We conclude that overexpression of Usp25m, sortilin, and GLUT4 leads directly to cleavage of endogenous TUG proteins and can redistribute GLUT4 and IRAP in nonadipocyte cells.

We wondered whether reduced insulin-stimulated TUG cleavage contributes to insulin resistance in adipose tissue. To test this idea, we first used a short-term dietary intervention, in which rats treated for 3 days with a high-fat, high-sugar (HFS) diet were compared with those maintained on regular chow (RC). This brief dietary manipulation was sufficient to cause increased fasting blood glucose and insulin concentrations, as shown in Fig. 8, *A* and *B*. Because the glucose and insulin measurements were paired, we calculated HOMA-IR, a measure of insulin resistance. This measurement confirmed that the short-term HFS diet resulted in whole-body insulin resistance (Fig. 8*C*). Furthermore, the ability of insulin to suppress plasma nonesterified fatty acid concentrations was impaired in the HFS-fed animals (Fig. 8*D*). Because these fatty acids derive primarily from lipolysis in adipose tissue, the data support the idea that the diet caused an impairment of insulin action in adipocytes.

To assess insulin-stimulated TUG proteolysis in adipose tissue, we immunoblotted GWAT lysates prepared from fasting and acutely insulin-stimulated, RC-fed, and HFS-fed rats. As shown in Fig. 8*E*, insulin stimulated the depletion of intact TUG protein in adipose tissue from RC-fed rats, and this effect was not observed in HFS-fed animals. The C-terminal cleavage products were not observed in rat adipose lysates, possibly because of differences in methods of sample preparation for GWAT, compared with 3T3-L1 adipocytes. Nonetheless, the insulin-stimulated decrease in intact TUG abundance was dramatic. We quantified this effect relative to an α-tubulin loading control, as shown in Fig. 8*F*. In GWAT from RC-fed animals, insulin stimulated an ~60% decrease in the abundance of intact TUG. In contrast, no insulin-stimulated change in TUG abundance was observed in GWAT from HFS-fed rats. The data support the idea that in adipose tissue, insulin-stimulated TUG cleavage is impaired by a brief HFS-diet treatment in rats.

We examined whether the 3-day HFS diet impaired insulin signaling through PI3K to Akt. As shown in Fig. 8*G*, insulin stimulated the phosphorylation of Akt at Ser-473 similarly in GWAT from RC- and HFS-fed animals. These data were quantified for several fasted and insulin-treated animals in each group in Fig. 8*H*. As shown, insulin-stimulated Akt phosphorylation was robust on both diets, and there was no impairment of Akt signaling by this short-term treatment with the HFS diet. We conclude that in rats, brief HFS-diet treatment resulted in insulin resistance and impaired TUG cleavage in GWAT, and this occurred in the absence of a discernable defect in insulin signaling to Akt.

To learn whether Usp25m abundance is reduced by the HFS diet, we performed immunoblots of GWAT from RC- and HFS-fed rats. Fig. 8*I* shows that Usp25m was dramatically reduced in the HFS-fed animals, compared with RC-fed controls. The data were quantified in Fig. 8*J*, which shows that, on average, Usp25m abundance in GWAT was reduced by ~60% by 3 days on the HFS diet. Therefore, together the data support the idea that short-term dietary manipulation can cause insulin resistance in rats, which involves GWAT and is characterized by impaired TUG proteolysis and reduced Usp25m abundance, and that this can occur in the absence of any large effect on insulin signaling to Akt.

We considered that the dietary manipulation would have to be maintained for more than 3 days to result in impaired insulin signaling through Akt, which is observed in many but not all insulin-resistant models (16). Therefore, to study whether signaling through TUG is also attenuated in the setting of a more established diet-induced insulin-resistant model, we examined GWAT of mice that had been placed on a high-fat diet (HFD) for 3 weeks, compared with control animals maintained on an RC diet. This dietary intervention induces marked whole-body insulin resistance, as we and others have observed previously using hyperinsulinemic clamps (10). Mice were fasted, treated with intraperitoneal injections of insulin/glucose solution or saline control, and sacrificed. As shown in Fig. 9*A*, insulin stimulated the acute depletion of intact TUG in GWAT of RC-fed mice but not in GWAT from HFD-fed animals. In RC-fed mice, intact TUG abundance was reduced by ~60%, similar to the data from rats (Fig. 9*B*, compare with Fig. 8*F*, above). In HFD-fed animals, the abundance of intact TUG was reduced at baseline, and there was no significant further effect of insulin. To test whether the reduction in TUG in the HFD animals results from a transcriptional effect, we used quantitative RT-PCR (Q-PCR) to assess the abundances of TUG mRNA. As shown in Fig. 9*C*, no reduction in TUG mRNA abundance was observed in GWAT from HFD-fed mice, compared with RC-fed controls. In addition, the data confirm that the reduction in intact TUG abundance observed after brief insulin stimulation is not related to reduced mRNA abundance. We observed an insulin-stimulated increase in the abundance of the 42-kDa C-terminal TUG cleavage product in RC-fed mice (Fig. 9*A*). We quantified the ratio of this product to total TUG and observed a significant increase after insulin stimulation in RC-fed but not HFD-fed mice (Fig. 9*D*). We also immunoblotted phospho-Akt (Ser-473) and total Akt, as shown in Fig. 9*A* and quantified in *E*. As expected, we observed a marked reduction in insulin-stimulated Akt phosphorylation in HFD-fed mice, compared with RC-fed controls. The data show that reduced TUG proteolytic processing and reduced Akt phosphorylation occur concurrently in adipose tissue of mice fed a HFD for 3 weeks, compared with those maintained on regular chow.

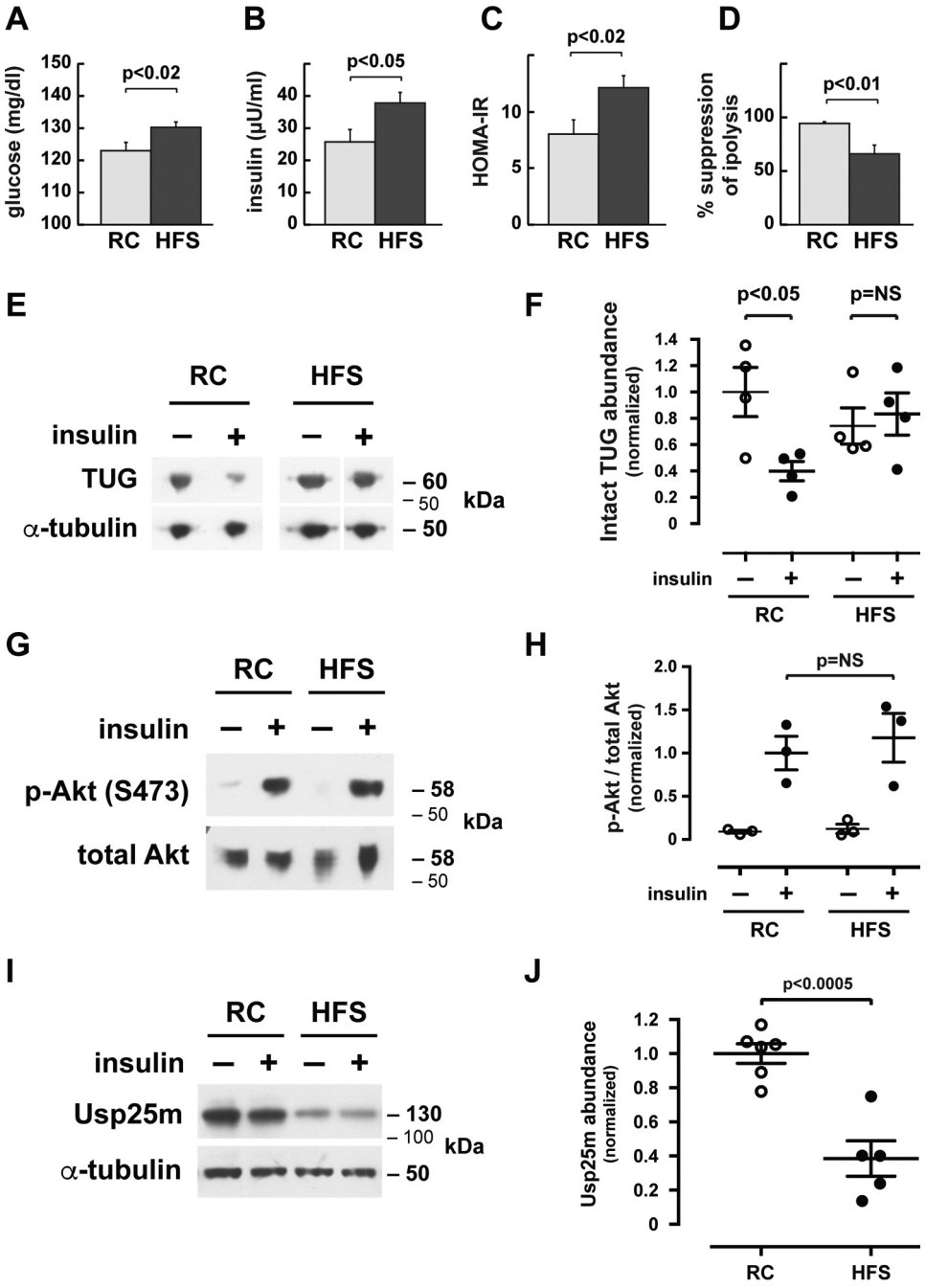

Figure 8. TUG processing, but not Akt phosphorylation, is impaired in adipose tissue of rats fed a 3-day high-fat diet. *A–D,* rats were fed RC or HFS diet for 3 days, as described under "Experimental procedures." Fasting plasma glucose (*A*) and insulin (*B*) were measured, and HOMA-IR (*C*) was calculated ($n = 15$ and 20 for RC and HFS groups, respectively). To calculate the percent suppression of lipolysis (*D*), rats were treated with a primed–continuous infusion of insulin and glucose (to prevent hypoglycemia) for 20 min, and plasma nonesterified fatty acids were measured before and after the infusion ($n = 7$ and 9 in RC and HFS groups, respectively). *E–J,* gonadal white adipose tissue from RC-fed or HFS-fed, fasted, or 20-min insulin-stimulated rats was immunoblotted to detect intact TUG (*E*), phospho-Akt (*G*), and Usp25m (*I*). Replicate samples from separate rats were quantified in *F, H,* and *J*, respectively. *NS*, not significant.

Immunoblots demonstrated that Usp25m abundance was dramatically reduced in GWAT from the HFD-fed mice, compared with RC-fed control animals, as shown in Fig. 9*A*. Data from several mice were quantified in Fig. 9*F*, which shows that in HFD-fed mice Usp25m abundance was decreased by ~80% compared with its abundance in RC-fed controls. We also observed a trend toward reduced Usp25m abundance after insulin treatment in RC-fed animals (Fig. 9*A*). This effect was not robustly observed in rat adipose tissue nor in 3T3-L1 adipocytes, in the data shown above. The HFD-induced reduction in Usp25m protein was quite marked, and we used Q-PCR to quantify *Usp25* mRNA abundance in GWAT of HFD- and RC-fed mice. As shown in Fig. 9*G*, no change in the abundance of *Usp25* mRNA was observed. As positive controls, we also quantified mRNAs for *Ppargc1a*, *Pck1*, and *Adipoq*; these were significantly (*Ppargc1a* and *Pck1*) or nearly significantly (*Adipoq*) reduced in HFD-fed animals, as expected. Therefore, we conclude that HFD-induced insulin resistance is associated with

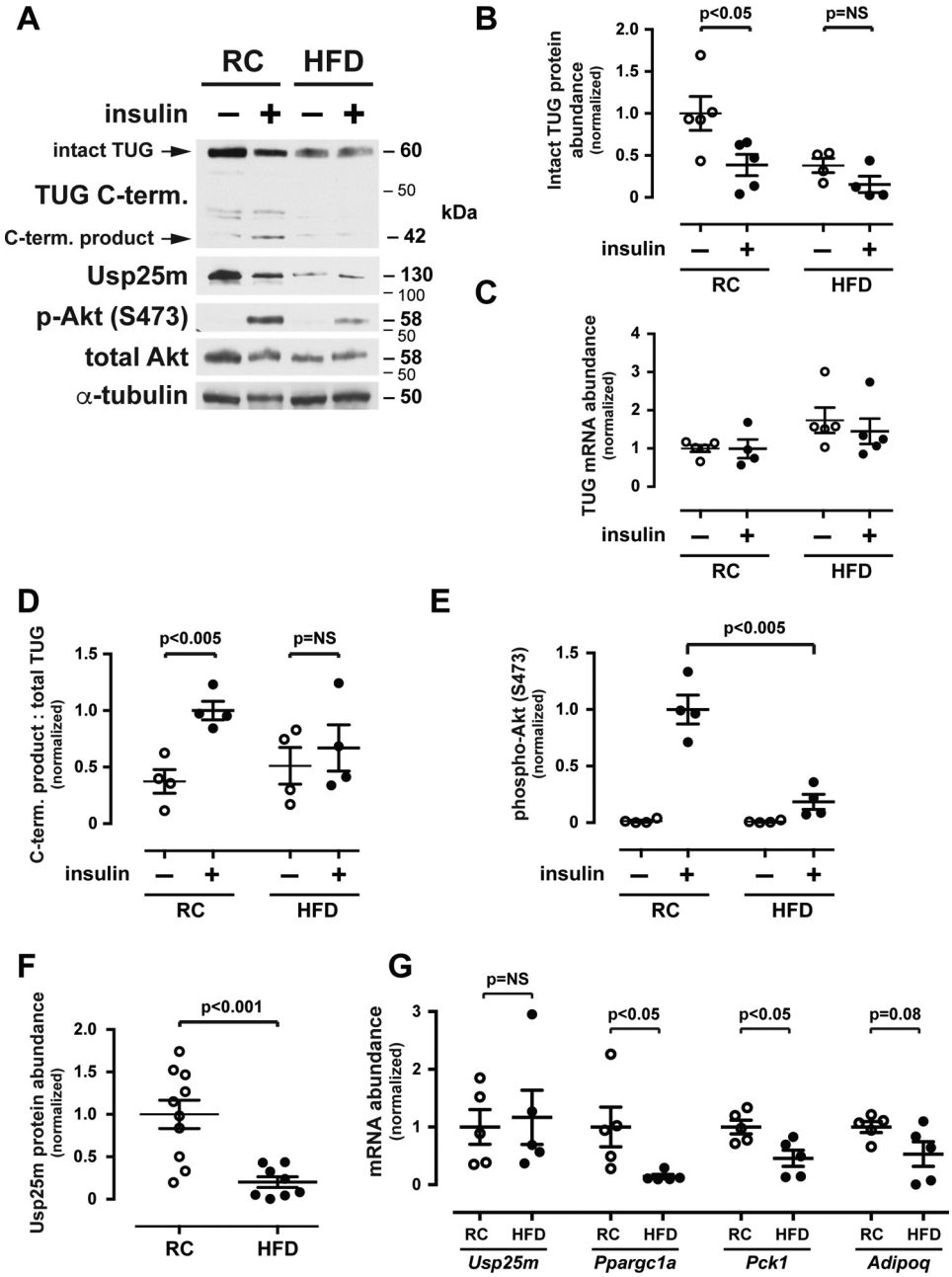

Figure 9. Both TUG processing and Akt phosphorylation are impaired in adipose tissue of mice fed a 3-week high-fat diet. *A,* mice were maintained on RC or fed a HFD for 3 weeks, as described under "Experimental procedures." Mice were fasted for 4–6 h and treated by intraperitoneal injection of insulin/glucose solution or saline control. After 30 min, mice were sacrificed; lysates were prepared from gonadal white adipose tissue, and immunoblots were done as indicated. *B,* replicate immunoblots were quantified, and the relative abundances of intact TUG were plotted. *C,* Q-PCR was used to quantify the relative abundances of TUG mRNA in the samples used in *A*. *NS*, not significant. *D* and *E,* replicate immunoblots were quantified, and the ratio of abundances of the TUG C-terminal product to intact TUG (*D*) and of phospho-Akt (*E*) were quantified. *F,* immunoblots were done to quantify the relative abundance of Usp25 in gonadal white adipose tissue of HFD-fed animals, compared with RC-fed controls. The loading control was α-tubulin. *G,* relative abundances of the indicated mRNAs were measured in gonadal white adipose tissue using Q-PCR.

reduced Usp25m protein, but not mRNA, in adipocytes. This may reflect accelerated degradation or reduced translation of the Usp25m protein, and it is accompanied by attenuated insulin-stimulated proteolytic processing of TUG proteins in adipocytes. These effects can occur together with reduced signaling to Akt. However, they can also occur before reduced insulin-stimulated Akt phosphorylation becomes apparent, early after dietary intervention to cause insulin resistance in rodents.

Discussion

Our results define a proteolytic mechanism for insulin action in adipocytes. The data support a model, depicted in Fig. 10, in which insulin stimulates the activity of Usp25m to cleave TUG, which liberates GSVs from the Golgi matrix and produces the ubiquitin-like protein modifier TUGUL. TUGUL then links the GSVs to its target substrate, KIF5B, and promotes GSV movement to the cell surface. Release of the vesicles from the Golgi is

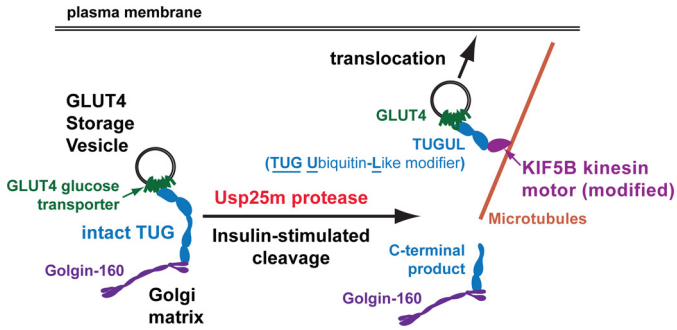

Figure 10. Model for GLUT4 storage vesicle mobilization. GSVs are retained intracellularly by intact TUG proteins, which link these vesicles to Golgi matrix proteins, including Golgin-160. Insulin stimulates the activity of Usp25m protease to cleave TUG. This liberates the vesicles from the Golgi matrix. The N-terminal TUG cleavage product, TUGUL, is a ubiquitin-like protein modifier that is attached covalently to KIF5B, a kinesin motor protein. Because TUGUL binds noncovalently to GSV proteins, including GLUT4, this loads the vesicle onto the motor to promote its translocation to the plasma membrane.

thus coupled to activation of a mechanism to promote their movement to the plasma membrane. This proteolytic pathway is independent of insulin signaling through the PI3K–Akt pathway, and it is impaired in adipose tissue of rodents with diet-induced insulin resistance.

Our data shed light on the cell-type specificity of insulin action. We observe dramatic up-regulation of Usp25m abundance during 3T3-L1 adipocyte differentiation and show that it is expressed in primary adipocytes as well as in muscle. Our data demonstrate that Usp25m is present on TUG-bound vesicles, that it associates with TUG and GLUT4 in unstimulated cells, and that it is released from this complex into the cytosol upon insulin addition. Usp25m was required for both TUG cleavage and GLUT4 translocation. Remarkably, Usp25m, but not Usp25a, catalyzed TUG cleavage in cotransfection experiments. This effect of transfected Usp25m was enhanced by coexpression of sortilin, another protein induced during adipocyte differentiation, which is essential for the formation of GSVs (5, 28, 34, 35). It is formally possible that Usp25m acts on another upstream target involved in GSV budding. Yet, sortilin is sufficient to cause budding of GSV-like vesicles in nonadipocytes, and we observed a minimal effect of sortilin to cause TUG cleavage in the absence of Usp25m. Thus, the simplest interpretation of the data is that sortilin acts to assemble a protein complex that facilitates Usp25m-mediated TUG proteolysis and that Usp25m acts directly to cleave TUG.

We do not know how Usp25m protease activity may be stimulated by an insulin signal. Our data show that insulin-stimulated TUG cleavage is independent of PI3K. This observation is consistent with previous results showing that TUG cleavage requires an insulin signal transduced by the TC10α GTPase and its effector protein, PIST, which binds directly to TUG (10, 13). This signaling pathway acts in parallel to the well-characterized PI3K–Akt–AS160 pathway (26, 36–40). We show here that both pathways converge, because AS160 was present on TUG-bound vesicles. It has been argued that the Akt pathway is sufficient to mediate insulin action, and this pathway has been the focus of substantial work on insulin resistance (41, 42). Yet, neither isolated PI3K activation nor isolated Akt activation fully mimics insulin action in 3T3-L1 adipocytes, and TC10α is required for GLUT4 translocation and glucose uptake (43, 44). We previously proposed that PIST inhibits the TUG protease in unstimulated cells and that activation of TC10α relieves this inhibitory effect (9, 10). Understanding how PIST interacts with a TUG-containing protein complex and how it may regulate Usp25m activity will require further study.

Previous work on GLUT4 trafficking revealed a "quantal release" mechanism, whereby increasing doses of insulin cause a stepwise increase in the number of GLUT4 molecules that recycle at the cell surface (45). In 3T3-L1 adipocytes, this mechanism is not observed when cells are replated for experiments (46). Our data support the idea that Usp25m mediates this quantal release of GLUT4 by catalyzing a dose-dependent increase in TUG cleavage (Fig. 3*B*). Importantly, the release of GSVs from intact TUG can account for the bulk of insulin action during maximal stimulation of 3T3-L1 adipocytes (7, 8) and in quadriceps muscles *in vivo* (10). In muscle, this pathway coordinately regulates distinct physiological effects of GLUT4 and of IRAP, supporting its central importance (11). Previous data further show how insulin sensitivity may be modulated by NAD^+ through SIRT2, which controls TUG acetylation (and possibly acylation) to control the accumulation of GSVs in unstimulated cells (12). Presumably, Usp25m can act only on complexes containing acetylated TUG, because mutation of the acetylated residues disrupted cleavage, but how this occurs is not understood.

In 3T3-L1 adipocytes, GSVs are mobilized directly to the cell surface at 3–6 min after insulin addition, but the GSV cargoes recycle through endosomes at ≥15 min after insulin addition (8). These data are consistent with the quantal release of GSVs and dose-dependence of TUG cleavage, noted above. The idea that GSVs are released at the transition from the basal to insulin-stimulated state also fits well with the observation that in acutely stimulated 3T3-L1 cells, TC10α activation is very transient (44). Together with other data, this transient activation led us to propose that this signaling pathway contains an upstream feed-forward circuit (9, 47). According to this model, Usp25m activation and TUG cleavage are coupled to acute changes (*e.g.* fold-increases) in insulin concentrations, not to absolute (or steady state) insulin concentrations. Physiologically, TUG cleavage and GSV mobilization would then be proportional to glycemic load (1, 9).

Our data show that insulin stimulates the conjugation of TUGUL to KIF5B. This result builds on previous data showing that TUGUL functions as a ubiquitin-like protein modifier (13, 30). Although we do not identify the site of KIF5B modification, our data show that the TUGUL–KIF5B complex was resistant to denaturing lysis, that RNAi-mediated depletion of KIF5B caused depletion of the TUGUL-modified protein, and that TUGUL and KIF5B colocalized in 3T3-L1 adipocytes. KIF5B tugulation was wortmannin-insensitive, similar to KIF5B-mediated GLUT4 movement (29). Other enzymes involved in TUGUL modification are unknown, although Ubc9 binds GLUT4 and regulates its trafficking and may function as a TUGUL-conjugating enzyme in this context (48–50). Our data show that insulin stimulates the association of GLUT4 with KIF5B and that Usp25m and TUG processing are required for this effect. The data support the idea that TUGUL, which binds

noncovalently to GLUT4 and IRAP, is covalently attached to KIF5B to load the GSVs onto this motor. Recently, the importance of KIF5B *in vivo* was demonstrated using adipose tissue-specific knockout mice, which have increased adiposity and insulin resistance, compared with controls, when treated with a high-fat diet (51). Our data show that TUG processing is reduced in adipocytes of insulin-resistant rodents, supporting the pathophysiological significance of this KIF5B knockout model. The data both emphasize the potential role of this processing pathway in human insulin resistance and also identify ubiquitin-like modification as a novel biochemical mechanism by which cargo can be loaded onto a kinesin motor.

Our present data do not indicate whether Usp25m mediates TUG cleavage and glucose uptake in muscle, as in adipose tissue. Our previous data show that in muscle, TUG is cleaved in response to insulin (10, 12) and during cardiac ischemia/reperfusion (52). Data indicate that the cleavage site is identical to that in adipocytes, and it seems most likely that Usp25m catalyzes TUG cleavage in muscle cells, as well as adipocytes. How the 70 additional residues (out of 1125 total) present in Usp25m, but not Usp25a, confer a specific function to cleave TUG is also uncertain (23, 24). The Usp25a splice form functions in inflammation (53–56), cancer (57), endoplasmic reticulum-associated degradation (58, 59), and Wnt signaling (60). In general, Usp25 proteins contain three ubiquitin-binding domains near the N terminus, which can bind the small ubiquitin-like modifier (SUMO) as well as ubiquitin (22, 61). Recent work shows that two of these, a pair of tandem ubiquitin-interacting motifs, bind Lys-48–linked ubiquitin chains (62). Possibly, in Usp25m these motifs interact with tandem ubiquitin-like folds in TUGUL (13, 30). All Usp25 isoforms bind tankyrase *in vitro* through the R*XX*PDG-like motif present at the Usp25 C terminus (17). Yet, the function of tankyrase in GLUT4 regulation is not well-understood and cannot be due solely to scaffolding of IRAP and Usp25m in proximity, because data imply that the poly(ADP-ribosylation) activity of tankyrase is involved (18, 19, 63). In skeletal muscle, Usp25m interacts with sarcomeric proteins (24). Understanding whether these proteins act during muscle contraction to promote Usp25m-mediated TUG cleavage and GLUT4 translocation will require substantial further study.

Our data show that in rodents with diet-induced insulin resistance, TUG proteolysis is impaired in epididymal white adipose tissue. In rats treated with the diet for only 3 days, this effect was observed in the absence of a defect in insulin-stimulated Akt phosphorylation, suggesting that the Usp25m–TUG pathway is impaired early during the development of diet-induced insulin resistance in adipose tissue. Supporting this idea, we observed substantially decreased Usp25m protein abundance in the insulin-resistant animals, compared with controls. This observation can account for how reduced effects of insulin can be observed, independently of Akt signaling, in settings of overnutrition (16). After a more prolonged 3-week high-fat diet in mice, both Usp25m–TUG and PI3K–Akt signaling were reduced in GWAT. Thus, insulin signaling through both of these pathways can be impaired concurrently in rodents with diet-induced insulin resistance. Intriguingly, the abundance of Usp25m protein, but not mRNA, was reduced in adipose tissue of the insulin-resistant mice. It seems likely that degradation of the Usp25m protein is accelerated in the setting of high-fat diet-induced insulin resistance. Of note, previous data show that rats with diet- or ethanol-induced insulin resistance have impaired signaling through TC10α (64, 65). Thus, alterations in this signaling mechanism may occur at multiple levels and may act independently of the Akt pathway during the development of insulin resistance.

Together with previous results, we conclude that Usp25m-mediated proteolysis of TUG proteins is an important mechanism for the regulation of GLUT4 translocation and glucose uptake in adipocytes. The results define a novel ubiquitin-like processing pathway, which links insulin action with kinesin-mediated vesicle transport. The data show that this pathway is impaired early during the development of insulin resistance in adipose tissue and that it is independent of insulin signaling through Akt. A full understanding of the molecular regulation of this Usp25m–TUG pathway will require substantial future work. Nonetheless, results presented here provide an improved understanding of insulin action and how it may be impaired in obesity and diabetes.

Experimental procedures

Reagents and cell culture

Polyclonal rabbit antisera directed to the TUG N and C termini were described previously (6, 12). Splenocytes from an animal immunized to generate the TUG N-terminal antisera were used to isolate a rabbit mAb, termed 10–10 (Epitomics, Inc.). A rabbit polyclonal antibody was also raised to the first ubiquitin-like domain of TUG (30) and was used for immunoprecipitation. Antibodies to GLUT4 and IRAP were described previously (12, 27). Other antibodies were purchased, including those directed to β-actin (ThermoFisher Scientific, catalog no. MA5-15739); Usp25 (Abcam ab187156 and Novus NBP180631); Myc epitope tag (Sigma E6654 and clone 9E10 from Developmental Studies Hybridoma Bank); IRAP (clone D7C5, Cell Signaling Technology 6918S); VAMP2 (clone D6O1A, Cell Signaling 13508S); VAMP3 (Abcam ab5789); LRP1 (clone EPR3724, Abcam ab92544); acetyl-CoA-carboxylase (Cell Signaling 3662S); AS160 (clone C69A7, Cell Signaling 2670S); α-tubulin (Sigma T5168); β-tubulin (Developmental Studies Hybridoma Bank clone E7-b); phospho-Ser-473; and total Akt (clones D9E and C67E7, Cell Signaling 4060S and 4691S); KIF5B (Abcam ab167429 (clone EPR10276(B)); and Millipore MAB1614 (clone H2)); transferrin receptor (Abcam ab84036); insulin receptor β-chain (Millipore 07-724); and sortilin (Abcam ab16640). GFP-trap affinity matrix was purchased from Chromotek, GmbH, and anti-Myc affinity matrix was purchase from Sigma. Plasmids to express myc-Usp25a and myc-Usp25m were the kind gifts of Dr. Gemma Marfany (22). A plasmid to express sortilin-myc/His was a kind gift of Dr. Konstantin Kandror (28). A plasmid to express FLAG-AS160 was a kind gift of Dr. Gustav Lienhard (66). Chemicals were obtained from Sigma unless otherwise noted.

3T3-L1, HEK293, and HeLa cells were cultured in high-glucose DMEM GlutaMAX medium (Invitrogen) containing 10% bovine growth serum (HyClone) and plasmocin (Invivogen).

3T3-L1 adipocytes were differentiated in 10% fetal bovine serum with supplements, as described previously (12). To express exogenous proteins or shRNAs, 3T3-L1 cells were infected with retroviruses and selected using puromycin and FACS (67). Control cells containing nontargeting shRNAs or empty vector were also subjected to puromycin selection; together with plasmocin, this helped to maintain cells free of mycoplasma. Expression of shRNAs was done using the pSIREN-RetroQ vector (Clontech) as described previously (12). The Usp25 shRNAs targeted the following sequences: 5′-GCACAGAAATAGAGAAATA-3′ (shRNA#1); 5′-GAAGAAACGCTCCGAGTGA-3′ (shRNA#2); 5′-GCACGAACTCTGTGAGCGA-3′ (shRNA#3); 5′-CCTGCTGGTTTAGTGCAGTTA-3′ (shRNA#4); and 5′-CCCAACGATCACTGCAAGAAA-3′ (shRNA#5). Lipofectamine 2000 (Invitrogen) was used for transient transfection of HEK293 and HeLa cells.

For transient transfection of synthetic siRNA duplexes in 3T3-L1 adipocytes, a modification of the protocol described by Kilroy *et al.* (68) was used. Briefly, for each 10-cm plate of cells, Lipofectamine 2000 (10 μl) and DMEM (250 μl) were incubated 5 min at room temperature as were siRNA (25 μg) and DMEM (250 μl). The Lipofectamine and siRNA mixtures were then combined and incubated 20 min at room temperature. 3T3-L1 adipocytes at day 7 of differentiation were resuspended using trypsin. Trypsin was quenched in 3 ml of DMEM, 10% fetal bovine serum, and cells were transferred to 15-ml tubes. Cells were centrifuged at 1000 rpm for 5 min, and excess media were aspirated. The siRNA mixture was diluted to 10 ml and used to resuspend the cells. The cell suspension was incubated for 10 min at room temperature and then replated onto the original 10-cm dishes. Cells were cultured for an additional 48 h and then starved 3 h prior to treatment with or without insulin. After stimulation, media were aspirated; cells were rinsed with ice-cold PBS and then lysed in 1% Nonidet P-40 buffer with vortexing every 5 min for 20 min SDS-PAGE and immunoblotting were performed using Invitrogen NuPAGE 4–12% bis-tris gels, as described below. The siRNA duplexes targeting KIF5B were purchased from Thermo Dharmacon (option A4, 2′-deprotected, duplexed; UU overhangs) and the sense strands were as follows: KIF5B siRNA#1, 5′-GCAGUUGGUACGCGAUAAU-3′; KIF5B siRNA#2, 5′-GACCUCUCAACGAAUCUGA-3′. Control experiments used mock transfections and nontargeting siRNAs, as described previously (13).

Western blots, immunoprecipitation

For experiments using basal and insulin-stimulated 3T3-L1 adipocytes, cells were typically serum-starved for 3 h prior to insulin stimulation. Insulin was used at 80–160 nM for 15–30 min unless otherwise specified. Lysis was done in TNET buffer as described (12), except that 1% Nonidet P-40 was used instead of 1% Triton X-100. SDS-PAGE and immunoblots were performed as described previously (12). Images were acquired on film using enhanced chemiluminescence (Pierce) or by IR detection using an LI-COR Odyssey imaging station. Densitometry of films was done using transillumination on an Epson Perfection V700 scanner, and quantification was done using ImageJ.

Immunoprecipitations were done using the lysis buffer above for nondenaturing conditions. For denaturing conditions, cells were lysed at 95 °C using 1% SDS, 50 mM Tris, pH 7.4, 150 mM NaCl, 2 mM EDTA, 20 mM iodoacetamide (Sigma), and complete protease inhibitor tablets (Roche Applied Science; 1 tablet/20 ml). After needle shearing of DNA and pelleting of insoluble debris, lysates were diluted 5-fold using 1% Nonidet P-40 in phosphate-buffered saline (PBS). Immunoprecipitating antibody was added, and incubations were allowed to proceed overnight at 4 °C, and then protein A-Sepharose beads were added for an additional 4 h at 4 °C. For immunoprecipitations using GFP-trap or antibodies to epitope tags, affinity matrices were incubated overnight with cell lysates. For GFP-trap, Nonidet P-40 was used at 0.5%. After pelleting in a benchtop microcentrifuge, beads were washed six times with 1 or 0.5% Nonidet P-40 buffer and transferred to new tubes. Samples were eluted by heating (5 min, 95 °C) in SDS-PAGE sample buffer with 10% 2-mercaptoethanol or without heat using glycine buffer, pH 2.5, with neutralization by Tris base, pH 9. Samples were separated on 4–12% NuPAGE bis-tris gels and immunoblotted as above.

Subcellular fractionation, vesicle purification, biotinylation of cell-surface proteins

Subcellular fractionation was performed as described previously (7, 12, 27). Briefly, for each sample, five 10-cm plates of 3T3-L1 adipocytes were homogenized in 5 ml of an ice-cold TES buffer (250 mM sucrose, 10 mM Tris, pH 7.4, 0.5 mM EDTA, protease inhibitor mixture, and 20 mM iodoacetamide) using a glass Dounce-type homogenizer. PM, LM, HM, M/N, and cytosolic fractions were isolated by differential centrifugation (7, 12, 27). Pellets were resuspended in SDS-PAGE sample buffer with 10% 2-mercaptoethanol. Samples were heated for 5 min at 95 °C, separated on 4–12% bis-tris gels, transferred to nitrocellulose membranes, and immunoblotted as above.

Lipid rafts were isolated by a modification of established protocols (69, 70). Briefly, 3T3-L1 adipocytes were serum-starved, treated with or without insulin (160 nM insulin, 7–10 min), then placed on ice, and washed with cold PBS. For each sample, three 10-cm plates were lysed in a total of 2 ml of 0.4% Triton X-100 in MES-buffered saline (25 mM MES, pH 6.5, 150 mM NaCl, 2 mM EDTA). Lysates were passed five times through a 23-gauge needle, incubated for 10 min on ice with periodic inversion, and mixed with 2 ml of 80% sucrose, so that the final sucrose concentration was 40% in MES-buffered saline. Samples were transferred to 12-ml centrifuge tubes and overlaid with 6 ml of 30% sucrose and 2 ml of 5% sucrose to produce a discontinuous gradient. Samples were centrifuged in an SW-41 rotor for 18 h at 37,500 rpm. Fractions of 1 ml each were taken from the top of the gradient and analyzed by immunoblotting.

TUG-bound vesicles were purified from cell homogenates by using a form of TUG containing a C-terminal biotin tag, as described (11). Briefly, retroviruses were used to express both TUG containing a biotin acceptor peptide as well as the BirA-biotinylating enzyme in 3T3-L1 cells. After differentiation into adipocytes, cells were serum-starved, treated with or without insulin (160 nM, 15 min), homogenized in TES buffer (above), and incubated with streptavidin-agarose beads (Neutravidin, Pierce). Biotin-saturated streptavidin beads were used as a con-

trol. Beads were pelleted and washed, and proteins were eluted and analyzed by SDS-PAGE and immunoblotting. The endogenous biotinylated protein, acetyl-CoA carboxylase, was used as a control to demonstrate that purification of biotinylated proteins was similar in basal and insulin-stimulated cells. Biotinylation of cell-surface proteins was done using sulfo-NHS–SS–biotin (Pierce) as described previously (11, 12). After cell lysis, biotinylated proteins were purified using streptavidin beads, eluted, and analyzed by SDS-PAGE as described above.

Confocal microscopy

3T3-L1 adipocytes were serum-starved, treated with or without insulin (160 nM, 15 min), and fixed for 5–10 min using 4% paraformaldehyde (Electron Microscopy Sciences). Cells were permeabilized, and nonspecific staining was blocked using 4% bovine serum albumin (BSA), 5% normal goat serum, and 0.1% Triton X-100 for 30 min. The TUG N terminus was stained using a rabbit mAb (10-10), Usp25m was stained using a rabbit polyclonal antibody (Abcam), and KIF5B was stained using a mouse mAb (Millipore). All primary antibodies were used at 1:100 in 5% normal goat serum overnight, and control experiments omitted primary antibody. After three washes of 5 min each using PBS, cells were incubated with a 1:200 dilution of Alexa488-conjugated goat anti-mouse IgG secondary antibody and/or Alexa568-conjugated goat anti-rabbit IgG secondary antibody (Invitrogen) for 2 h. After three further washes of 5 min with PBS, cells were mounted using ProLong Gold (Invitrogen). Images were acquired on a Leica SP5 confocal microscope using a ×63 oil immersion objective with the pinhole set at 1 Airy unit. For microscopy of unpermeabilized cells, to detect Myc-tagged GLUT4 at the cell surface, cells were not fixed, and all steps were performed at 4 °C. After blocking with 4% BSA and 5% normal goat serum, cell surface Myc was detected using 9E10 antibody (Covance) at 1:100 for 1 h. Cells were washed three times briefly using PBS, and then incubated with Alexa568-conjugated goat anti-mouse IgG secondary antibody for 1 h. After a further three brief washes in PBS, cells were mounted and imaged as above.

For images of basal and insulin-stimulated cells expressing GLUT4–GFP together with WT TUG or exogenous TUG GGVV, cells were treated with 160 nmol of insulin for >15 min, so that GLUT4 redistribution reached steady state in WT cells (27). All images were acquired using the Airyscan detector on a Zeiss LSM 880 confocal microscope equipped with a stage incubator (37 °C, 5% CO_2) and an α Plan-Apochromat ×100/1.46 NA objective. Airyscan deconvolution was performed using the default (Auto Filter) in the SR Mode of ZEN (Zeiss). Images were acquired using 4-line averaging with very low incident laser power ranging from 0.8% (225 nW/cm^2) to 1.0% (297 nW/cm^2, measured at the sample) to minimize photodamage.

Insulin titration and wortmannin treatment

Fully differentiated 3T3-L1 adipocytes in 10-cm dishes were serum-starved and then washed with PBS. Insulin was added at the specified concentrations to 10 ml of pre-warmed DMEM in separate tubes, which were then mixed and added to each plate. Usp25 shRNA#1 and shRNA#3 cells were treated concurrently using the maximal concentration of insulin. After 30 min at 37 °C, media were aspirated and cells were rinsed with ice-cold PBS prior to lysis. Samples were lysed using 1% Nonidet P-40 buffer, above, for 20 min on ice with vortexing every 5 min. Sample buffer was added, and samples were heated to 95 °C for 5 min and analyzed by SDS-PAGE and immunoblotting.

For experiments using wortmannin, 3T3-L1 adipocytes were starved for 3 h prior to insulin stimulation. Control and Usp25 shRNA#1 3T3-L1 adipocytes were used. Relative to the time of cell lysis ($t = 0$), cells were treated with or without wortmannin (100 nM) at $t = -45$ min, and with or without insulin (160 nM) at $t = -30$ min. At $t = 0$, media were aspirated; cells were rinsed in ice-cold PBS, and cells were lysed using 1% Nonidet P-40 lysis buffer as above. After addition of sample buffer, samples were heated for 5 min at 95 °C and analyzed by SDS-PAGE and immunoblotting.

Animals

Animal protocols were approved by the Yale University Institutional Animal Care and Use Committee. All animals were housed at the Yale Animal Research Center under controlled temperature (22 ± 2 °C) and lighting (12 h of light, 0700–1900 h; 12 h of dark, 1900–0700 h) with free access to water and food. To assess Usp25m expression in adipose tissue, tissues were obtained from fasting 12-week-old male C57BL/6J mice (The Jackson Laboratory). After euthanasia, GWAT, quadriceps muscles, other hindlimb muscles, and brain were collected and flash-frozen in liquid nitrogen and stored at −80 °C. For immunoblots, tissues were quickly thawed, and 500 mg of each tissue were weighed and mixed with 1% Nonidet P-40 lysis buffer, above. A Qiagen TissueLyser II was used to grind the tissue for 3 min at 30 cycles/s. Lysates were centrifuged at 13,000 rpm in a tabletop centrifuge at 4 °C to remove insoluble debris. Supernatants were analyzed by SDS-PAGE and immunoblotting as above.

For studies of diet-induced insulin resistance in rats, male Sprague-Dawley rats were purchased from Charles River Laboratories at 350–450 g of body weight. Seven days before the study, animals had jugular venous and carotid arterial lines placed, and 3 days before the study they were placed on HFS diet or maintained on a control diet. The HFS diet consisted of Dyets no. 112245 (60% kcal from fat, 0–1% myristate, 5% palmitate, 2% stearate, 12% oleate, 80% linoleate) together with 6% w/v sucrose in the drinking water. The control diet was standard rodent chow (Harlan Teklad 2018S: 24% protein, 58% carbohydrate, 18% fat) without any sucrose added to the drinking water. On the morning of the study, all rats were fasted 6 h. Insulin-treated rats were given a 200-milliunit/kg insulin bolus followed by a 4-milliunit/(kg/min) continuous insulin infusion, together with 25 μl/min of 20% dextrose to prevent hypoglycemia, and were sacrificed after 20 min of insulin stimulation. Epididymal white adipose tissue was harvested, snap-frozen in liquid nitrogen-cooled tongs, and stored at −80 °C until analysis. Measurements of plasma glucose, insulin, and nonesterified fatty acid concentrations were performed as described (71). HOMA-IR was calculated from fasting plasma glucose and insulin concentrations, as [glucose]·[insulin]/

22.5, where glucose is expressed in mmol/liter and insulin is in milliunits/liter.

For studies of diet-induced insulin resistance in mice, 12–14-week-old male C57BL/6J mice were fed ResearchDiets D12492 (60% kcal from fat) or maintained on standard chow (Harlan-Teklad 2018S, above) for 3 weeks. Mice were fasted 4–6 h, then treated with intraperitoneal injection of insulin (8 units/kg) and glucose (1 g/kg), or an equivalent volume (0.3 ml) of PBS. After 30 min, mice were anesthetized and sacrificed by cervical dislocation. GWAT was excised, snap-frozen in liquid N_2, and stored at −80 °C. For immunoblots, lysis was in 1% Nonidet P-40 lysis buffer as above. For Q-PCR, a Macherey-Nagel Nucleospin RNA preparation kit was used. GWAT (100 mg) was lysed in 1 ml of buffer containing of 1% 2-mercaptoethanol and homogenized using 10 strokes in a 2-ml ground glass Dounce-type tissue grinder. After purification, RNA was eluted with water and quantified, and 670 nmol of RNA was used with a high-capacity cDNA reverse transcriptase kit (Applied Biosystems). Real-time PCR was done using a StepOnePlus system and Power SYBR Green Master Mix (Applied Biosystems). mRNA abundances were normalized to that for β-actin (*Actb*). Primers for *Usp25* were TCCGGCACCAAGGCACATCAC and ACGGCATGGAGGCGGTAAGG, and primers for *Actb* were TGGAATCCTGTGGCATCCATGAAAC and TAAAACGCAGCTCAGTAACAGTCCG. Primers for *Ppargc1a*, *Pck1*, and *Adipoq* were as described (72). In Q-PCR experiments, three technical replicates were done for each biological replicate; technical replicates typically agreed to 3–4 significant figures and were averaged. Biological replicates (from separate mice) are plotted and were used to compare chow and high-fat diet-fed mice.

Replicates and statistical analysis

All data were replicated in at least three independent experiments. For data presented in scatter plots or bar graphs, three or more biological replicates were analyzed, and data are presented as mean ± S.E. Biological replicates indicate that data were obtained using different mice or different plates of cultured cells. Significance was assessed using an unpaired, two-tailed *t* test or using one-way analysis of variance with Bonferroni adjustment for multiple comparisons of preselected pairs, and *p* values were indicated in the figures. Differences were considered significant at $p < 0.05$. For the bar graphs, *N* for each measurement is indicated in the figure legends. No statistical tool was used to pre-determine sample sizes; rather, the availability of materials and previous experience determined the number of biological replicates that were used. No blinding was done; no randomization was used, and no sample was excluded from analysis.

Author contributions—E. N. H., D. T. L., and J. S. B. conceptualization; E. N. H., D. T. L., X. O. W., M. L., M. C. P., H. L., S. G. D., E. L., O. J.-Z., and J. S. W. validation; E. N. H., D. T. L., A. A.-R., X. O. W., M. L., M. C. P., H. L., S. G. D., E. L., O. J.-Z., J. S. W., and J. S. B. investigation; E. N. H., D. T. L., X. O. W., M. L., M. C. P., H. L., S. G. D., E. L., O. J.-Z., J. S. W., and J. S. B. methodology; E. N. H., D. T. L., and J. S. B. writing-review and editing; A. A.-R. and M. C. P. resources; A. A.-R. and J. S. B. data curation; J. S. B. formal analysis; J. S. B. supervision; J. S. B. funding acquisition; J. S. B. writing-original draft; J. S. B. project administration.

Acknowledgments—We thank Dr. Gerald Shulman, Dr. Nai-Wen Chi, Arielle Patterson, Vincent Calia-Bogan, and Roland Calia-Bogan for helpful discussions and assistance, and Dr. Gemma Marfany, Dr. Konstantin Kandror, and Dr. Gustav Lienhard for kindly sharing plasmids. This work used the Cell Biology Core of the Yale Diabetes Endocrinology Research Center (supported by National Institutes of Health Grant P30 DK45735) as well as services provided by the W. M. Keck Foundation Biotechnology Resource Laboratory at Yale University.

References

1. Bogan, J. S. (2012) Regulation of glucose transporter translocation in health and diabetes. *Annu. Rev. Biochem.* **81,** 507–532 CrossRef Medline
2. Xu, Z., and Kandror, K. V. (2002) Translocation of small preformed vesicles is responsible for the insulin activation of glucose transport in adipose cells. Evidence from the *in vitro* reconstitution assay. *J. Biol. Chem.* **277,** 47972–47975 CrossRef Medline
3. Bogan, J. S., and Kandror, K. V. (2010) Biogenesis and regulation of insulin-responsive vesicles containing GLUT4. *Curr. Opin. Cell Biol.* **22,** 506–512 CrossRef Medline
4. Kandror, K. V., and Pilch, P. F. (2011) The sugar is sIRVed: sorting Glut4 and its fellow travelers. *Traffic* **12,** 665–671 CrossRef Medline
5. Huang, G., Buckler-Pena, D., Nauta, T., Singh, M., Asmar, A., Shi, J., Kim, J. Y., and Kandror, K. V. (2013) Insulin responsiveness of glucose transporter 4 in 3T3-L1 cells depends on the presence of sortilin. *Mol. Biol. Cell* **24,** 3115–3122 CrossRef Medline
6. Bogan, J. S., Hendon, N., McKee, A. E., Tsao, T. S., and Lodish, H. F. (2003) Functional cloning of TUG as a regulator of GLUT4 glucose transporter trafficking. *Nature* **425,** 727–733 CrossRef Medline
7. Yu, C., Cresswell, J., Löffler, M. G., and Bogan, J. S. (2007) The glucose transporter 4-regulating protein TUG is essential for highly insulin-responsive glucose uptake in 3T3-L1 adipocytes. *J. Biol. Chem.* **282,** 7710–7722 CrossRef Medline
8. Xu, Y., Rubin, B. R., Orme, C. M., Karpikov, A., Yu, C., Bogan, J. S., and Toomre, D. K. (2011) Dual-mode of insulin action controls GLUT4 vesicle exocytosis. *J. Cell Biol.* **193,** 643–653 CrossRef Medline
9. Belman, J. P., Habtemichael, E. N., and Bogan, J. S. (2014) A proteolytic pathway that controls glucose uptake in fat and muscle. *Rev. Endocr. Metab. Disord.* **15,** 55–66 CrossRef Medline
10. Löffler, M. G., Birkenfeld, A. L., Philbrick, K. M., Belman, J. P., Habtemichael, E. N., Booth, C. J., Castorena, C. M., Choi, C. S., Jornayvaz, F. R., Gassaway, B. M., Lee, H. Y., Cartee, G. D., Philbrick, W., Shulman, G. I., Samuel, V. T., and Bogan, J. S. (2013) Enhanced fasting glucose turnover in mice with disrupted action of TUG protein in skeletal muscle. *J. Biol. Chem.* **288,** 20135–20150 CrossRef Medline
11. Habtemichael, E. N., Alcázar-Román, A., Rubin, B. R., Grossi, L. R., Belman, J. P., Julca, O., Löffler, M. G., Li, H., Chi, N. W., Samuel, V. T., and Bogan, J. S. (2015) Coordinated regulation of vasopressin inactivation and glucose uptake by action of TUG protein in muscle. *J. Biol. Chem.* **290,** 14454–14461 CrossRef Medline
12. Belman, J. P., Bian, R. R., Habtemichael, E. N., Li, D. T., Jurczak, M. J., Alcázar-Román, A., McNally, L. J., Shulman, G. I., and Bogan, J. S. (2015) Acetylation of TUG protein promotes the accumulation of GLUT4 glucose transporters in an insulin-responsive intracellular compartment. *J. Biol. Chem.* **290,** 4447–4463 CrossRef Medline
13. Bogan, J. S., Rubin, B. R., Yu, C., Löffler, M. G., Orme, C. M., Belman, J. P., McNally, L. J., Hao, M., and Cresswell, J. A. (2012) Endoproteolytic cleavage of TUG protein regulates GLUT4 glucose transporter translocation. *J. Biol. Chem.* **287,** 23932–23947 CrossRef Medline
14. Govers, R. (2014) Cellular regulation of glucose uptake by glucose transporter GLUT4. *Adv. Clin. Chem.* **66,** 173–240 CrossRef Medline
15. Klip, A., Sun, Y., Chiu, T. T., and Foley, K. P. (2014) Signal transduction meets vesicle traffic: the software and hardware of GLUT4 translocation. *Am. J. Physiol. Cell Physiol.* **306,** C879–C886 CrossRef Medline

16. Czech, M. P. (2017) Insulin action and resistance in obesity and type 2 diabetes. *Nat. Med.* **23,** 804–814 CrossRef Medline
17. Sbodio, J. I., and Chi, N. W. (2002) Identification of a tankyrase-binding motif shared by IRAP, TAB182, and human TRF1 but not mouse TRF1. NuMA contains this *RXX*PDG motif and is a novel tankyrase partner. *J. Biol. Chem.* **277,** 31887–31892 CrossRef Medline
18. Yeh, T. Y., Sbodio, J. I., Tsun, Z. Y., Luo, B., and Chi, N. W. (2007) Insulin-stimulated exocytosis of GLUT4 is enhanced by IRAP and its partner tankyrase. *Biochem. J.* **402,** 279–290 CrossRef Medline
19. Zhong, L., Ding, Y., Bandyopadhyay, G., Waaler, J., Börgeson, E., Smith, S., Zhang, M., Phillips, S. A., Mahooti, S., Mahata, S. K., Shao, J., Krauss, S., and Chi, N. W. (2016) The PARsylation activity of tankyrase in adipose tissue modulates systemic glucose metabolism in mice. *Diabetologia* **59,** 582–591 CrossRef Medline
20. Guo, H. L., Zhang, C., Liu, Q., Li, Q., Lian, G., Wu, D., Li, X., Zhang, W., Shen, Y., Ye, Z., Lin, S. Y., and Lin, S. C. (2012) The Axin/TNKS complex interacts with KIF3A and is required for insulin-stimulated GLUT4 translocation. *Cell Res.* **22,** 1246–1257 CrossRef Medline
21. Yeh, T. Y., Beiswenger, K. K., Li, P., Bolin, K. E., Lee, R. M., Tsao, T. S., Murphy, A. N., Hevener, A. L., and Chi, N. W. (2009) Hypermetabolism, hyperphagia, and reduced adiposity in tankyrase-deficient mice. *Diabetes* **58,** 2476–2485 CrossRef Medline
22. Denuc, A., Bosch-Comas, A., Gonzàlez-Duarte, R., and Marfany, G. (2009) The UBA-UIM domains of the USP25 regulate the enzyme ubiquitination state and modulate substrate recognition. *PLoS One* **4,** e5571 CrossRef Medline
23. Valero, R., Bayés, M., Francisca Sánchez-Font, M., González-Angulo, O., Gonzàlez-Duarte, R., and Marfany, G. (2001) Characterization of alternatively spliced products and tissue-specific isoforms of USP28 and USP25. *Genome Biol.* **2,** RESEARCH0043 Medline
24. Bosch-Comas, A., Lindsten, K., Gonzàlez-Duarte, R., Masucci, M. G., and Marfany, G. (2006) The ubiquitin-specific protease USP25 interacts with three sarcomeric proteins. *Cell. Mol. Life Sci.* **63,** 723–734 CrossRef Medline
25. Jedrychowski, M. P., Gartner, C. A., Gygi, S. P., Zhou, L., Herz, J., Kandror, K. V., and Pilch, P. F. (2010) Proteomic analysis of GLUT4 storage vesicles reveals LRP1 to be an important vesicle component and target of insulin signaling. *J. Biol. Chem.* **285,** 104–114 CrossRef Medline
26. Larance, M., Ramm, G., Stöckli, J., van Dam, E. M., Winata, S., Wasinger, V., Simpson, F., Graham, M., Junutula, J. R., Guilhaus, M., and James, D. E. (2005) Characterization of the role of the Rab GTPase-activating protein AS160 in insulin-regulated GLUT4 trafficking. *J. Biol. Chem.* **280,** 37803–37813 CrossRef Medline
27. Bogan, J. S., McKee, A. E., and Lodish, H. F. (2001) Insulin-responsive compartments containing GLUT4 in 3T3-L1 and CHO cells: regulation by amino acid concentrations. *Mol. Cell. Biol.* **21,** 4785–4806 CrossRef Medline
28. Shi, J., and Kandror, K. V. (2005) Sortilin is essential and sufficient for the formation of Glut4 storage vesicles in 3T3-L1 adipocytes. *Dev. Cell* **9,** 99–108 CrossRef Medline
29. Semiz, S., Park, J. G., Nicoloro, S. M., Furcinitti, P., Zhang, C., Chawla, A., Leszyk, J., and Czech, M. P. (2003) Conventional kinesin KIF5B mediates insulin-stimulated GLUT4 movements on microtubules. *EMBO J.* **22,** 2387–2399 CrossRef Medline
30. Tettamanzi, M. C., Yu, C., Bogan, J. S., and Hodsdon, M. E. (2006) Solution structure and backbone dynamics of an N-terminal ubiquitin-like domain in the GLUT4-regulating protein, TUG. *Protein Sci.* **15,** 498–508 CrossRef Medline
31. Johnson, E. S., Bartel, B., Seufert, W., and Varshavsky, A. (1992) Ubiquitin as a degradation signal. *EMBO J.* **11,** 497–505 Medline
32. Johnson, E. S., Ma, P. C., Ota, I. M., and Varshavsky, A. (1995) A proteolytic pathway that recognizes ubiquitin as a degradation signal. *J. Biol. Chem.* **270,** 17442–17456 CrossRef Medline
33. Johnston, S. C., Larsen, C. N., Cook, W. J., Wilkinson, K. D., and Hill, C. P. (1997) Crystal structure of a deubiquitinating enzyme (human UCH-L3) at 1.8 A resolution. *EMBO J.* **16,** 3787–3796 CrossRef Medline
34. Shi, J., Huang, G., and Kandror, K. V. (2008) Self-assembly of Glut4 storage vesicles during differentiation of 3T3-L1 adipocytes. *J. Biol. Chem.* **283,** 30311–30321 CrossRef Medline
35. Pan, X., Zaarur, N., Singh, M., Morin, P., and Kandror, K. V. (2017) Sortilin and retromer mediate retrograde transport of Glut4 in 3T3-L1 adipocytes. *Mol. Biol. Cell* **28,** 1667–1675 CrossRef Medline
36. Chen, Y., Wang, Y., Zhang, J., Deng, Y., Jiang, L., Song, E., Wu, X. S., Hammer, J. A., Xu, T., and Lippincott-Schwartz, J. (2012) Rab10 and myosin-Va mediate insulin-stimulated GLUT4 storage vesicle translocation in adipocytes. *J. Cell Biol.* **198,** 545–560 CrossRef Medline
37. Karunanithi, S., Xiong, T., Uhm, M., Leto, D., Sun, J., Chen, X. W., and Saltiel, A. R. (2014) A Rab10:RalA G protein cascade regulates insulin-stimulated glucose uptake in adipocytes. *Mol. Biol. Cell* **25,** 3059–3069 CrossRef Medline
38. Sano, H., Eguez, L., Teruel, M. N., Fukuda, M., Chuang, T. D., Chavez, J. A., Lienhard, G. E., and McGraw, T. E. (2007) Rab10, a target of the AS160 Rab GAP, is required for insulin-stimulated translocation of GLUT4 to the adipocyte plasma membrane. *Cell Metab.* **5,** 293–303 CrossRef Medline
39. Sano, H., Roach, W. G., Peck, G. R., Fukuda, M., and Lienhard, G. E. (2008) Rab10 in insulin-stimulated GLUT4 translocation. *Biochem. J.* **411,** 89–95 CrossRef Medline
40. Brewer, P. D., Habtemichael, E. N., Romenskaia, I., Mastick, C. C., and Coster, A. C. (2016) Glut4 is sorted from a Rab10 GTPase-independent constitutive recycling pathway into a highly insulin-responsive Rab10 GTPase-dependent sequestration pathway after adipocyte differentiation. *J. Biol. Chem.* **291,** 773–789 CrossRef Medline
41. Ng, Y., Ramm, G., Lopez, J. A., and James, D. E. (2008) Rapid activation of Akt2 is sufficient to stimulate GLUT4 translocation in 3T3-L1 adipocytes. *Cell Metab.* **7,** 348–356 CrossRef Medline
42. Samuel, V. T., and Shulman, G. I. (2016) The pathogenesis of insulin resistance: integrating signaling pathways and substrate flux. *J. Clin. Invest.* **126,** 12–22 CrossRef Medline
43. Xu, Y., Nan, D., Fan, J., Bogan, J. S., and Toomre, D. (2016) Optogenetic activation reveals distinct roles of PIP3 and Akt in adipocyte insulin action. *J. Cell Sci.* **129,** 2085–2095 CrossRef Medline
44. Chang, L., Chiang, S. H., and Saltiel, A. R. (2007) TC10α is required for insulin-stimulated glucose uptake in adipocytes. *Endocrinology* **148,** 27–33 CrossRef Medline
45. Govers, R., Coster, A. C., and James, D. E. (2004) Insulin increases cell surface GLUT4 levels by dose dependently discharging GLUT4 into a cell surface recycling pathway. *Mol. Cell. Biol.* **24,** 6456–6466 CrossRef Medline
46. Muretta, J. M., Romenskaia, I., and Mastick, C. C. (2008) Insulin releases Glut4 from static storage compartments into cycling endosomes and increases the rate constant for Glut4 exocytosis. *J. Biol. Chem.* **283,** 311–323 CrossRef Medline
47. Hart, Y., and Alon, U. (2013) The utility of paradoxical components in biological circuits. *Mol. Cell* **49,** 213–221 CrossRef Medline
48. Giorgino, F., de Robertis, O., Laviola, L., Montrone, C., Perrini, S., McCowen, K. C., and Smith, R. J. (2000) The sentrin-conjugating enzyme mUbc9 interacts with GLUT4 and GLUT1 glucose transporters and regulates transporter levels in skeletal muscle cells. *Proc. Natl. Acad. Sci. U.S.A.* **97,** 1125–1130 CrossRef Medline
49. Lalioti, V. S., Vergarajauregui, S., Pulido, D., and Sandoval, I. V. (2002) The insulin-sensitive glucose transporter, GLUT4, interacts physically with Daxx. Two proteins with capacity to bind Ubc9 and conjugated to SUMO1. *J. Biol. Chem.* **277,** 19783–19791 CrossRef Medline
50. Liu, L. B., Omata, W., Kojima, I., and Shibata, H. (2007) The SUMO conjugating enzyme Ubc9 is a regulator of GLUT4 turnover and targeting to the insulin-responsive storage compartment in 3T3-L1 adipocytes. *Diabetes* **56,** 1977–1985 CrossRef Medline
51. Cui, J., Pang, J., Lin, Y. J., Gong, H., Wang, Z. H., Li, Y. X., Li, J., Wang, Z., Jiang, P., Dai, D. P., Li, J., Cai, J. P., Huang, J. D., and Zhang, T. M. (2017) Adipose-specific deletion of Kif5b exacerbates obesity and insulin resistance in a mouse model of diet-induced obesity. *FASEB J.* **31,** 2533–2547 CrossRef Medline
52. Quan, N., Sun, W., Wang, L., Chen, X., Bogan, J. S., Zhou, X., Cates, C., Liu, Q., Zheng, Y., and Li, J. (2017) Sestrin2 prevents age-related intolerance to

ischemia and reperfusion injury by modulating substrate metabolism. *FASEB J.* **31,** 4153–4167 CrossRef Medline

53. Lin, D., Zhang, M., Zhang, M. X., Ren, Y., Jin, J., Zhao, Q., Pan, Z., Wu, M., Shu, H. B., Dong, C., and Zhong, B. (2015) Induction of USP25 by viral infection promotes innate antiviral responses by mediating the stabilization of TRAF3 and TRAF6. *Proc. Natl. Acad. Sci. U.S.A.* **112,** 11324–11329 CrossRef Medline
54. Ren, Y., Zhao, Y., Lin, D., Xu, X., Zhu, Q., Yao, J., Shu, H. B., and Zhong, B. (2016) The type I interferon-IRF7 axis mediates transcriptional expression of Usp25 gene. *J. Biol. Chem.* **291,** 13206–13215 CrossRef Medline
55. Zhong, B., Liu, X., Wang, X., Chang, S. H., Liu, X., Wang, A., Reynolds, J. M., and Dong, C. (2012) Negative regulation of IL-17-mediated signaling and inflammation by the ubiquitin-specific protease USP25. *Nat. Immunol.* **13,** 1110–1117 CrossRef Medline
56. Zhong, H., Wang, D., Fang, L., Zhang, H., Luo, R., Shang, M., Ouyang, C., Ouyang, H., Chen, H., and Xiao, S. (2013) Ubiquitin-specific proteases 25 negatively regulates virus-induced type I interferon signaling. *PLoS One* **8,** e80976 CrossRef Medline
57. Li, J., Tan, Q., Yan, M., Liu, L., Lin, H., Zhao, F., Bao, G., Kong, H., Ge, C., Zhang, F., Yu, T., Li, J., He, X., and Yao, M. (2014) miRNA-200c inhibits invasion and metastasis of human non-small cell lung cancer by directly targeting ubiquitin specific peptidase 25. *Mol. Cancer* **13,** 166 CrossRef Medline
58. Blount, J. R., Burr, A. A., Denuc, A., Marfany, G., and Todi, S. V. (2012) Ubiquitin-specific protease 25 functions in endoplasmic reticulum-associated degradation. *PLoS One* **7,** e36542 CrossRef Medline
59. Jung, E. S., Hong, H., Kim, C., and Mook-Jung, I. (2015) Acute ER stress regulates amyloid precursor protein processing through ubiquitin-dependent degradation. *Sci. Rep.* **5,** 8805 CrossRef Medline
60. Xu, D., Liu, J., Fu, T., Shan, B., Qian, L., Pan, L., and Yuan, J. (2017) USP25 regulates Wnt signaling by controlling the stability of tankyrases. *Genes Dev.* **31,** 1024–1035 CrossRef Medline
61. Meulmeester, E., Kunze, M., Hsiao, H. H., Urlaub, H., and Melchior, F. (2008) Mechanism and consequences for paralog-specific sumoylation of ubiquitin-specific protease 25. *Mol. Cell* **30,** 610–619 CrossRef Medline
62. Kawaguchi, K., Uo, K., Tanaka, T., and Komada, M. (2017) Tandem UIMs confer Lys48 ubiquitin chain substrate preference to deubiquitinase USP25. *Sci. Rep.* **7,** 45037 CrossRef Medline
63. Chi, N. W., and Lodish, H. F. (2000) Tankyrase is a Golgi-associated mitogen-activated protein kinase substrate that interacts with IRAP in GLUT4 vesicles. *J. Biol. Chem.* **275,** 38437–38444 CrossRef Medline
64. Jun, H. S., Hwang, K., Kim, Y., and Park, T. (2008) High-fat diet alters PP2A, TC10, and CIP4 expression in visceral adipose tissue of rats. *Obesity* **16,** 1226–1231 CrossRef Medline
65. Sebastian, B. M., and Nagy, L. E. (2005) Decreased insulin-dependent glucose transport by chronic ethanol feeding is associated with dysregulation of the Cbl/TC10 pathway in rat adipocytes. *Am. J. Physiol. Endocrinol. Metab.* **289,** E1077–E1084 CrossRef Medline
66. Sano, H., Kane, S., Sano, E., Mîinea, C. P., Asara, J. M., Lane, W. S., Garner, C. W., and Lienhard, G. E. (2003) Insulin-stimulated phosphorylation of a Rab GTPase-activating protein regulates GLUT4 translocation. *J. Biol. Chem.* **278,** 14599–14602 CrossRef Medline
67. Liu, X., Constantinescu, S. N., Sun, Y., Bogan, J. S., Hirsch, D., Weinberg, R. A., and Lodish, H. F. (2000) Generation of mammalian cells stably expressing multiple genes at predetermined levels. *Anal. Biochem.* **280,** 20–28 CrossRef Medline
68. Kilroy, G., Burk, D. H., and Floyd, Z. E. (2009) High efficiency lipid-based siRNA transfection of adipocytes in suspension. *PLoS One* **4,** e6940 CrossRef Medline
69. Brown, D. A., and Rose, J. K. (1992) Sorting of GPI-anchored proteins to glycolipid-enriched membrane subdomains during transport to the apical cell surface. *Cell* **68,** 533–544 CrossRef Medline
70. Scherer, P. E., Lisanti, M. P., Baldini, G., Sargiacomo, M., Mastick, C. C., and Lodish, H. F. (1994) Induction of caveolin during adipogenesis and association of GLUT4 with caveolin-rich vesicles. *J. Cell Biol.* **127,** 1233–1243 CrossRef Medline
71. Vatner, D. F., Majumdar, S. K., Kumashiro, N., Petersen, M. C., Rahimi, Y., Gattu, A. K., Bears, M., Camporez, J. P., Cline, G. W., Jurczak, M. J., Samuel, V. T., and Shulman, G. I. (2015) Insulin-independent regulation of hepatic triglyceride synthesis by fatty acids. *Proc. Natl. Acad. Sci. U.S.A.* **112,** 1143–1148 CrossRef Medline
72. Liu, S., Kim, T. H., Franklin, D. A., and Zhang, Y. (2017) Protection against high-fat-diet-induced obesity in MDM2(C305F) mice due to reduced p53 activity and enhanced energy expenditure. *Cell Rep.* **18,** 1005–1018 CrossRef Medline